Barley guanine nucleotide exchange factor *Hv*GEF14 is an activator of the susceptibility factor *Hv*RACB and supports host cell entry by *Blumeria graminis* f.sp. *hordei*

Adriana Trutzenberg[1], Stefan Engelhardt[1], Ralph Hückelhoven[1,2]

[1] Chair of Phytopathology, TUM School of Life Sciences, Technical University of Munich

[2] corresponding author

Email addresses: a.trutzenberg@tum.de; stefan1.engelhardt@tum.de; hueckelhoven@tum.de

Chair of Phytopathology

TUM School of Life Sciences
Technische Universität München
Emil-Ramann-Str. 2
D-85354 Freising

Tel.: +49 8161 71-3681
Fax: +49 8161 71-4538

Date of submission: 04.08.2021
Number of Figures: 8
Word count: 6185
Number of Supplementary Figures: 8
Number of Supplementary Tables: 7

Running title

*Hv*GEF14 activates *Hv*RACB in barley epidermis

Highlight

The activated GTPase *Hv*RACB is a susceptibility factor of barley in response to *Blumeria graminis* f.sp. *hordei*. The newly discovered guanine nucleotide exchange factor *Hv*GEF14 is a *Hv*RACB activator.

Abstract

In barley (*Hordeum vulgare*), the function of ROPs appears central to polar cell development and the interaction outcome with parasitic fungi but little is known about ROP activation. Guanine nucleotide exchange factors (GEFs) facilitate the exchange of GDP with GTP and thereby turn ROPs into a signalling-activated ROP-GTP state. Plants possess a unique class of GEFs harbouring a plant specific ROP nucleotide exchanger domain (PRONE). We performed phylogenetic analyses and annotated barley PRONE GEFs. *HvGEF14* is expressed in leaf epidermal tissue and downregulated after inoculation with *Blumeria graminis* f.sp. *hordei*. Protein-protein interaction assays indicate that *Hv*GEF14 and the type I barley ROP protein *Hv*RACB can interact in yeast and *in planta*. Overexpression of *Hv*GEF14 further recruited the ROP-GTP downstream interactor *Hv*RIC171 to the cell periphery and let to interaction of *Hv*RACB with an extended CRIB (Cdc42/Rac Interactive Binding motif) peptide of *Hv*RIC171 in a similar manner as constitutively activated *Hv*RACB. Finally, the over expression of *HvGEF14* led to enhanced susceptibility to fungal entry while *HvGEF14* RNAi provoked a trend to more penetration resistance. *Hv*GEF14 might therefore play a role in the activation of *Hv*RACB in barley epidermal cells, which is crucial for fungal penetration success.

48 Keywords: barley, epidermis, fluorescence lifetime imaging, plant specific ROP nucleotide

49 exchanger, penetration resistance, powdery mildew, Rho of plants

50

51 ## Abbreviations:

52 ROP- Rho of plants

53 GEF- Guanine nucleotide exchange factor

54 PRONE- plant specific ROP-nucleotide exchanger

55 CA- constitutively activated

56 DN- dominant negative

57 GAP- GTPase activating protein

58 RIC- ROP interacting and CRIB domain containing protein

59 RIP- ROP interactive partner

60 GDI- Guanine nucleotide dissociation inhibitor

61 *Bgh- Blumeria graminis* forma specialis *hordei*

62 DH-PH- diffuse B-cell lymphoma homology – pleckstrin homology

63 DHR2- DOCK homology region 2

64 RLK- receptor like kinase

65 FER- FERONIA

66 *Hv- Hordeum vulgare*

67 *At- Arabidopsis thaliana*

68 Os- *Oryza sativa*

69 *Nb- Nicotiana benthamiana*

70 meGFP- monomeric enhanced green fluorescent protein

71 EV- empty vector

72 ## Introduction

73 In plants, cell polarity is central to cellular development and responses to external stimuli. ROPs (RHO
74 of plants) are small monomeric GTPases that function as signalling hubs regulating a multitude of cell
75 polarity processes that often involve cytoskeleton reorganization (Mucha *et al.*, 2011). Pollen tube
76 growth, the development of epidermal pavement cells and root hairs, but also processes that are
77 vital during plant-microbe interactions are examples for ROP-regulated processes (Engelhardt *et al.*,
78 2020; Zheng and Yang, 2000). ROPs are considered molecular switches due to their ability to shuttle
79 between a signalling-inactive, GDP-bound state, and a signalling-activated GTP-bound state (Bloch
80 and Yalovsky, 2013). An interaction with downstream signalling partners, and therefore signal
81 transduction, only occurs in the GTP-bound state (Nagawa, Xu, and Yang 2010). Certain point
82 mutations can lock ROPs in either the GTP-bound (constitutively activated (CA)) or GDP-bound
83 (dominant negative (DN)) conformation. Manipulating ROP downstream signalling in such a way can
84 lead to strong effects in a variety of polar growth processes. For example, *Arabidopsis thaliana*
85 ROP6^{DN} expressing plants show severe developmental phenotypes as well as misshaping of pavement
86 cells, indicating the importance of ROP-regulated cell polarity (Poraty-Gavra *et al.*, 2013).
87 To locally interact with downstream signalling partners, ROPs require to be membrane-associated,
88 which is achieved by posttranslational lipid modifications. Based on the primary sequence in the C-
89 terminal part, ROPs can be divided into two groups that both undergo distinct lipidations: type I ROPs
90 contain a CaaL-prenylation motif, whereas type II ROPs are S-acylated via a GC-CG box. Type I ROPs
91 can also be additionally S-acylated in an activation dependent manner (Winge *et al.*, 2000; Yalovsky,
92 2015). Amongst others, ROP signalling targets the cytoskeleton (Chen and Friml, 2014). In barley, the
93 activation of ROP-signalling influences the organization of actin filaments as well as the organization
94 of microtubules via the interaction of activated ROPs with scaffold proteins and **M**icrotubule-
95 **A**ssociated ROP **GAP 1**, *Hv*MAGAP1 (Hoefle *et al.*, 2020; Opalski *et al.*, 2005).
96 Barley (*Hordeum vulgare* L. (*Hv*)) contains six ROPs, which include *Hv*RACB and *Hv*RACD of type I and
97 *Hv*RAC1, *Hv*RAC3, *Hv*ROP4, *Hv*ROP6 of type II (Schultheiss *et al.*, 2003). Studies using stable

98 transgenic barley plants overexpressing constitutively activated variants of either *Hv*RACB, *Hv*RAC1 or
99 *Hv*RAC3 indicated a role for these ROPs in root and shoot development (Pathuri *et al.*, 2008;
100 Schultheiss *et al.*, 2005). Transgenic plants are also characterized by increased epidermal cell
101 expansion and failure of polar growth in root hairs. Additionally, different susceptibility levels during
102 the interaction with fungal leaf pathogens such as *Blumeria graminis* f.sp. *hordei* (*Bgh*) and
103 *Magnaporthe oryzae* suggest an involvement during fungal penetration (Pathuri *et al.*, 2008).
104 *Hv*RACB in particular has been studied in some detail for its function in susceptibility to penetration
105 and accommodation of haustoria from *Bgh* (Engelhardt *et al.*, 2020). Stable transgenic *Hv*RACB RNAi
106 plants with reduced expression levels of *HvRACB* do not develop root hairs and produce less and
107 misshaped stomatal subsidiary cells, which normally result from polar cell division. At the same time,
108 both stable and transient silencing of *HvRACB* limits fungal penetration success. Hence, *Hv*RACB is
109 considered a key developmental protein that is co-opted by *Bgh* during pathogenesis (Scheler *et al.*,
110 2016; Schultheiss *et al.*, 2002). *Hv*RAC1 has also been implicated in the generation of membrane
111 domains enriched with the ROP-scaffolding protein *Hv*RIPa at sites of fungal attack. The two proteins
112 interact at the plasma membrane, and together with *Hv*MAGAP1 they provoke membrane
113 asymmetry and microtubule reorganization in the cell cortex (Hoefle *et al.*, 2020).
114 Due to the vast number of signalling processes ROPs are involved in, it is apparent that tight
115 regulation of these molecular switches is required to fine-tune the complex cellular mechanisms
116 following ROP activation. This regulation is largely controlled by three classes of regulatory proteins:
117 **G**uanine nucleotide **E**xchange **F**actors (GEF), **G**TPase **A**ctivating **P**roteins (GAP) and **G**uanine
118 nucleotide **D**issociation **I**nhibitors (GDI) (Nagawa *et al.*, 2010; Vetter and Wittinghofer, 2001; Zheng
119 and Yang, 2000). Besides downstream signalling interactors, activated ROPs are also targeted by
120 GAPs, which abolish ROP-GTP signalling by enhancing the intrinsically low GTPase activity. This leads
121 to GTP hydrolysis and therefore to switching to the GDP-bound, signalling-inactive state (Wu *et al.*,
122 2000). An example of this is *Hv*MAGAP1 which interacts with *Hv*RACB and *Hv*RAC1. The presumable
123 negative regulation of *Hv*RACB signalling activity by over-expression of *Hv*MAGAP1 correlates with
124 limiting *Bgh* penetration success (Hoefle *et al.*, 2011).

125 GDIs prevent GDP-bound ROPs from membrane association and sequester them in the cytosol by
126 masking the C-terminal prenyl modification, thereby precluding an interaction with downstream
127 interaction partners (Nibau *et al.*, 2006). Regarding ROP signalling, GEFs are considered ROP-
128 signalling activating proteins that interact with GDP-bound ROPs to induce a conformational change
129 facilitating the exchange of GDP with highly abundant GTP (Berken *et al.*, 2005; Thomas *et al.*, 2007;
130 Thomas *et al.*, 2009).
131 ROP-signalling activating GEFs can be divided into sub-groups based on their protein domain
132 structures and primary sequence. Mammalian GEFs possess two types of conserved functional
133 domains: **d**iffuse B-cell lymphoma **h**omology – **p**leckstrin **h**omology (DH-PH) and **D**OCK **h**omology
134 **r**egion **2** (DHR2) (Schmidt and Hall, 2002). In plants, there has only been one example of DH-PH GEFs
135 and several reports on DHR2-type GEFs. The *O. sativa* DH-PH GEFs *Os*SWAP70A and B interact with
136 *Os*RAC1 and perform nucleotide exchange via their DH domain in order to facilitate defence-related
137 signalling in response to chitin elicitation (Yamaguchi *et al.*, 2012). The same group also confirmed
138 the corresponding *A. thaliana* homolog *At*SWAP70 to be involved in plant defence signalling during
139 effector and pattern triggered immunity (Yamaguchi and Kawasaki, 2012).
140 An example of a DHR2 GEF in plants is the so called SPIKE-GEF which has initially been identified by a
141 forward genetic screen of *A. thaliana* mutants, in which the *spike1* mutant showed severe
142 developmental defects, including misshaped trichomes (Qiu *et al.*, 2002). More recently, *Lj*SPIKE1 has
143 been found to activate *Lj*ROP6 during the polar growth of infection threads in root hairs of the
144 legume *Lotus japonicus* (*Lj*) (Liu *et al.*, 2020).
145 In addition, plants have evolved a specific class of GEFs with a highly conserved **P**lant specific
146 Rac/**RO**p **N**ucleotide **E**xchanger (PRONE) domain (Berken *et al.*, 2005; Gu *et al.*, 2006). The family of
147 PRONE-GEFs in the model plant *A. thaliana* consists of 14 members that have been studied for their
148 function in various polar growth processes, plant development (Chang *et al.*, 2013; Chen *et al.*, 2011;
149 Gu *et al.*, 2006; Huang *et al.*, 2018a) and immunity (Qu *et al.*, 2017). So far, the PRONE domain is the
150 only identified conserved part of these proteins. This domain can be divided into three subdomains
151 that show a high level of sequence conservation. The PRONE domain contains several interfaces that

152 were shown to physically interact with ROPs in a heterotetrameric complex of two ROPs with two
153 PRONE-GEFs. After binding to ROPs, the PRONE domain facilitates a rearrangement of the GTPase
154 which leads to GDP release. Nucleotide-free ROPs and GEFs can further interact as a stable complex
155 (Berken *et al.*, 2005; Chang *et al.*, 2013; Gu *et al.*, 2006; Thomas *et al.*, 2007). The PRONE domain is
156 flanked by N- and C-terminal variable regions that likely possess regulatory functions. Especially the
157 C-terminal regulatory stretch is subject to phosphorylation by upstream **R**eceptor **L**ike **K**inases (RLK)
158 that have been implicated in developmental as well as immunity related signalling pathways (Fehér
159 and Lajkó, 2015). For instance, the C-terminus of *At*GEF12 has been reported to inhibit GEF function
160 and *At*GEF12 interacts with ROPs only after phosphorylation by the pollen RLK *At*PRK2 (Zhang and
161 McCormick, 2007). Another example of this interaction is the multifunctional RLK FERONIA (FER) that
162 interacts directly with *At*GEF14 in *A. thaliana*. Further downstream, *At*GEF14 interacts with *At*ROP6
163 which functions in polar growth of epidermal cells (Lin *et al.*, 2018) and together with *At*RIC1
164 facilitates microtubule organization in order to deal with mechanical stress (Tang *et al.*, 2021). In
165 barley, a number of RLKs are involved in susceptibility towards *Bgh* and their transcript levels are
166 partially influenced by the abundance and the activation status of *Hv*RACB (Schnepf *et al.*, 2018).
167 Furthermore, *At*GEF14 was shown to localize to the apical region of pollen tubes and interacts with
168 *At*ROP1, a regulator of pollen tube growth (Gu *et al.*, 2006). In roots, *At*GEF14 may be also involved in
169 polar growth processes. It accumulates at the root hair initiation site before being replaced by other
170 GEFs during the initiation and elongation phase (Denninger *et al.*, 2019).
171 Based on these first reports of PRONE GEFs in *A. thaliana*, plant specific GEFs have been identified in
172 many other species, including economically important crops like *Oryza sativa*, in which six of the 11
173 putative PRONE-GEFs have been studied in some detail. As in *A. thaliana*, *O. sativa* GEFs are also
174 important in floral organ development. *Os*GEF7B (*Os*GEF2 in other publications, see (Akamatsu *et al.*,
175 2015; Akamatsu *et al.*, 2013)), for example, has been shown to be an important regulator of the seed
176 setting rate by regulating downstream *Os*RAC GTPases (Huang *et al.*, 2018b). Moreover, four pollen-
177 specifically expressed GEFs have been reported with distinct localisations during the development of
178 pollen tubes (Kim *et al.*, 2020). *Os*GEF10 has been found to activate *Os*RAC1 in order to form small

179 cuticular papillae and to regulate early plant development (Yoo *et al.*, 2011). In addition, *Os*GEF1
180 interacts with OsCERK1, a central part of the rice chitin receptor complex, and activates *Os*RAC1 for
181 its function in defence of *M. oryzae* (Akamatsu *et al.*, 2013).
182 This work investigates barley PRONE-GEFs, focussing on *Hv*GEF14. We report that *Hv*GEF14 is
183 expressed in the leaf epidermis and downregulated after inoculation with *Bgh*. *Hv*GEF14 can bind
184 barley ROPs in yeast and *in planta* and may be involved in activation of disease susceptibility-
185 associated barley ROPs in leaf epidermal cells.
186

187 Materials and Methods

188 **Plant and pathogen propagation and maintenance**
189 Spring barley (*Hordeum vulgare, Hv*) cultivar Golden Promise (propagated in greenhouse) was grown
190 in a climate chamber at 20 °C, 50 % humidity and long-day conditions (16h light, 8h dark) for 7-8 days
191 in standard potting soil (Einheitserde Classic). *Blumeria graminis* f.sp. *hordei* race A6 (*Bgh*) was
192 maintained on 7- 21 days old *H. vulgare* cv. Golden Promise (propagated in field conditions) in a
193 climate chamber with 18 °C and 65 % humidity in long day conditions (16h light, 8h dark).
194

195 **Cloning procedure**
196 Open reading frames of *Hordeum vulgare* cv. Golden Promise genes were amplified from whole leaf
197 cDNA with primers (Tab. 5) designed based on sequences from the Barley Genome (International
198 Barley Genome Sequencing Consortium (2012)). Constructs were cloned into destination vectors
199 (Tab. 4) using BP and LR clonase following manufacturer's instructions (Invitrogen). Plasmids were
200 prepared via column purification (Machery Nagel).
201

202 **ML analysis and phylogenetic tree construction**
203 Muscle alignment of 14 *Arabidopsis thaliana*, 11 *Oryza sativa* (sequences downloaded from TAIR and
204 NCBI on 10.05.2021) and 11 *H. vulgare* PRONE-GEFs (MOREX genome version 3) was performed in

205 SeaView Software. A maximum likelihood (PhyML) analysis was performed with an LG model,
206 bootstraps with 100 replicate, model-given amino acid equilibrium frequencies, NNI tree searching
207 and five random starts. *O. sativa* PRONE-GEFs were annotated based on the *A. thaliana*
208 nomenclature and *H. vulgare* PRONE-GEFs were annotated according to their homologues in *O.*
209 *sativa*. The resulting TBE tree's design was further adjusted in InkScape.
210
211 **RNA extraction and cDNA synthesis**
212 Plant material from seven days old *H. vulgare* cv. Golden Promise was collected. In three biological
213 replicates, whole leaf and epidermal peels were cut and directly frozen in liquid N_2. Leaf tissue was
214 directly ground in a tissue lyser with glass beads. RNA was extracted with TRIzol according to the
215 protocol in (Chomczynski and Sachhi, 1987) and DNAseI digestion was performed. Total RNA was
216 visualized on 1% agarose gel and the concentration measured via spectrophotometer (NanoDrop).
217 Subsequently, cDNA synthesis was performed from 1 µg RNA with the QuantiTect Reverse
218 Transcription Kit (Quiagen) according to the supplier's protocol. cDNA from 1 µg RNA was diluted
219 1/10 for further analysis and stored at -20 °C. cDNA quality was controlled on 1% agarose gel and
220 visualised with Ethidium-Bromide staining under UV-excitation.
221
222 **qRT-PCR**
223 Appropriate primers for *HvGEF14* (HORVU6Hr1G068660.3, Tab. 5) were designed with Primer3Plus
224 (www.bioinformatics.nl/cgi-bin/primer3plus/primer3plus.cgi), secondary structure of primers was
225 checked with Thermo Multiple Primer Analyser
226 (https://www.thermofisher.com/de/de/home/brands/thermo-scientific/molecular-
227 biology/molecular-biology-learning-center/molecular-biology-resource-library/thermo-scientific-
228 web-tools/multiple-primer-analyzer.html) and specificity of the amplicon was tested via BLAST.
229 Primer efficiency and amplification factor was analysed by a standard curve of a three-step dilution
230 series. A calibration curve was calculated with -3.116 slope, r^2 of 0.951 and y-intercept at 29.58. The
231 power was determined via the online calculator "qPCR Efficiency Calculator" (Thermo Fischer). 10 µl

232 reactions were prepared with the Maxima 2xSYBR Green/ROX qPCR Master Mix (Thermo Scientific),
233 primers were added at 200nM concentration and 1 µl of 1/10 cDNA dilution was used. qRT-PCR was
234 run on Aria Mx3000 thermocycler (Agilent) with 40 cycles at 60°C annealing temperature for 10
235 seconds and 72°C elongation for 15 seconds and subsequent melting curve (65°C – 95°C) for quality
236 control. Measurements with melting curve peaks varying from all other samples were excluded and a
237 maximum difference of 0.5 Cq between technical replicates was allowed. There were no Cq values
238 detectable for NTC of the housekeeping gene and for *HvGEF14* a Cq of 36.67 was measured for NTC.
239 *HvUbiquitin* was measured as a housekeeping gene in all runs due to its reliable Cq values in all
240 samples that did not differ more than 2 Cq and successful usage in previous work (Schnepf *et al.*,
241 2018). Threshold values were exported from the AriaMx software (Agilent) and foldchanges were
242 calculated via the $2^{-\Delta\Delta Ct}$ method by Livak and Schmittgen (2001).
243
244 **Yeast-2-Hybrid**
245 Protein-protein interactions via yeast-two-hybrid (Y2H) assays were performed as described in the
246 Matchmaker protocol (Clontech). *Hv*RACB (amino acids 1- 193) and *Hv*RAC1 (amino acids 1-211) open
247 reading frames were cloned with a premature STOP codon to express truncated ROP proteins lacking
248 their C-terminal prenylation/acylation signal sequence to avoid membrane localisation in yeast cells.
249 *Saccharomyces cerevisiae* strain AH109 was transformed with pGBKT7 and pGADT7 plasmids (Tab. 4)
250 containing the specific gene of interest and cultivated for 3-6 days at 30°C on synthetic dropout
251 medium lacking amino acids leucine and tryptophan (SD-L-W) medium. 5ml of liquid SD-L-W medium
252 was inoculated with yeast colonies and, upon overnight cultivation at 30°C, dilutions were dropped
253 on SD-L-W and SD-L-W-H (SD lacking amino acids leucine, tryptophan, histidine) or SD-L-W-H-Ade (SD
254 lacking amino acids leucine, tryptophan, histidine and nucleotide adenosine) plates and incubated at
255 30°C until distinct colony growth.
256
257 **Protein extraction from yeast and *N. benthamiana***

258 Transformed yeast was cultured in 4 ml synthetic dropout medium lacking amino acids leucine and
259 tryptophane (SD-L-W) overnight and centrifuged at 4000g for 5 min at 4°C. Cells were washed in 100
260 µl 2 M LiAc and subsequently incubated for 5 min at room temperature in 100 µl 0.4 M NaOH. Pellets
261 were collected and 50 µl 4x SDS-sample buffer was added. After vortexing, samples were boiled at 95
262 °C for 5 min and shortly centrifuged before loading onto an SDS-gel (Zhang *et al.*, 2011).
263 3 leaf discs (12 mm tissue punch) were collected from *A. tumefaciens*-transformed *N. benthamiana*
264 leaves 48 hpt and directly frozen in liquid N_2. The frozen plant material was homogenised in a tissue
265 lyser with glass beads and 200 µl 4x SDS sample buffer was added. After vortexing, samples were
266 boiled at 95°C for 10 min and shortly centrifuged before loading onto an SDS-gel.
267
268 **SDS-PAGE and Western Blot**
269 Extracted proteins were separated by electrophoresis in a 12% acrylamide gel and blotted onto PVDF
270 membrane via semi-dry Western Blotting (protein extracted from yeast) or wet Western Blotting
271 (protein extracted from *N. benthamiana*). The membrane was blocked with 5% milk in PBS buffer and
272 incubated with specific antibodies (see figure legends). Proteins were detected by
273 chemiluminescence with SuperSignalTM West Dura or FEMTO Chemiluminescence- Substrate
274 (Thermo ScientificTM).
275
276 **Transient biolistic transformation of barley epidermal cells**
277 Barley cv. Golden Promise seven days old detached leaves were transformed by particle
278 bombardment as described previously (McCollum *et al.*, 2020). 2 µg of plasmid/transformation was
279 used in FRET-FLIM experiments. For fungal penetration efficiency experiments, 1 µg
280 plasmid/transformation for the gene of interest and 0.5 µg plasmid/transformation of
281 transformation marker (pUbi_GUSplus, Addgene, encoding ß-Glucuronidase) was applied.
282
283 ***A.tumefaciens* infiltration of *N. benthamiana* leaves**

284 *Agrobacterium tumefaciens* strain GV3101 carrying binary expression vectors pGWB containing
285 either meGFP-*Hv*RACB WT, meGFP-*Hv*RACB G15V (CA), GST-mCherry, *Hv*CRIB46-mCherry or 3xHA-
286 *Hv*GEF14 were infiltrated into five-week-old *N. benthamiana* leaves according to Yang *et al.* (2000).
287 Bacterial liquid cultures were grown to OD600 0.5 and mixed in equal amounts including P19
288 silencing suppressor. 48 hours after infiltration, proteins were extracted for Western Blotting and
289 FRET-FLIM measurements were performed on leaf discs.
290
291 **FRET-FLIM**
292 For protein-protein interaction studies, *Hv*GEF14 was N-terminally tagged with monomeric enhanced
293 GFP as donor and N-terminal fusions with mCherry of *Hv*RACB variants were used as acceptors.
294 To test *Hv*RACB activation status in planta, binary vectors of meGFP-*Hv*RACB WT or meGFP-*Hv*RACB
295 CA were co-expressed with GST-mCherry or *Hv*CRIB46-mCherry with or without co-expression of
296 3HA-*Hv*GEF14 via *A. tumefaciens* infiltration in *N. benthamiana* leaves.
297 Microscopy of transiently transformed *H. vulgare* epidermis cells and *A. tumefaciens*-infiltrated *N.*
298 *benthamiana* leave discs was performed with an Olympus FV 3000 microscope with 488 nm (20 mW)
299 and 561 nm (50 mW) diode lasers. GFP photons were excited with a 485 nm (LDH-D-C-485) pulsed
300 diode laser and time- correlated single photon counting (TCSPC) was performed with 2x PMA Hybrid
301 40 photon counting detectors. A minimum of 1000 photon counts were collected and subsequently
302 analysed with the PicoQuant SymPhoTime 64 software. N-exponential reconvolution and decay curve
303 fitting with daily measured or calculated IRF, for *H. vulgare* and *N. benthamiana* respectively, was
304 applied to gain a fit with X^2 values between 0.9 and 1.2.
305
306 **Confocal microscopy**
307 Transiently transformed barley epidermis cells were imaged 24 hours post transformation (hpt) with
308 a Leica TCS SP5 confocal microscope with hybrid HyD and PMT detectors. mCherry fluorophores
309 were excited with a 561nm laser and detected at 570-610nm. GFP fluorescence was excited with a
310 488nm Argon laser and detected between 500-550nm.

311

312 **RNAi efficiency**

313 GFP tagged *Hv*GEF14 was transiently over expressed together with overexpression of cytosolic
314 mCherry as a transformation marker. In addition, either the empty vector or a *HvGEF14* RNAi hairpin
315 construct of amino acids 201-401 was co-transformed and fluorescence intensity of GFP and mCherry
316 was measured in the z-stack of confocal images taken 48 hpt. RNAi efficiency was determined by the
317 ratio of mean mCherry-normalised GFP fluorescence in *HvGEF14* silenced cells divided by mCherry-
318 normalised GFP-*Hv*GEF14 expressing control cells.

319

320 **Fungal penetration efficiency assays**

321 Detached barley leaves were fixed on 0.8% H_2O-agar and inoculated 24 hours after transient
322 transformation with over-expression constructs or 48 hours after transient transformation with RNAi
323 constructs with roughly 100 *Bgh* conidiospores per mm^2. Inoculated leaves were incubated for 48
324 hours in a climate chamber with 18-22 °C under long day conditions (16h light, 8h dark). Inoculated
325 leaves were stained in X-Gluc (5-Bromo-4-chloro-3-indolyl ß-D-glucuronic acid) solution 48 hours
326 after inoculation and fixed in 80% EtOH. Fungal penetration efficiency (PE) was determined with light
327 microscopy as described in Hückelhoven *et al.* (2003).

328

329 **Statistical analysis**

330 Statistical analyses were performed in Rstudio. Global comparison for non-parametric data was
331 assessed with Kruskal.test() and pairwise comparisons of non-parametric data were calculated via
332 wilcox.test() with bonferroni p-value adjustment. Outlier tests were performed with grubbs.test().
333 Figures were prepared with RStudio's ggplot2 package and adjusted in InkScape.

334

335 # Results

336 **Phylogenetic analysis reveals three distinct clades of barley PRONE-GEFs**

337 To investigate guanine nucleotide exchange factors in barley, we concentrated on the well described
338 PRONE domain-containing class of exchange factors first introduced by Berken *et al.* (2005). In total,
339 we identified 11 PRONE domain-encoding genes in *Hordeum vulgare* cv. Morex genome version 3
340 (Mascher *et al.*, 2021). Using the MUSCLE algorithm, we aligned full-length primary amino acid
341 sequences of these 11 barley PRONE-GEFs (Tab. 2) with 11 PRONE-GEFs of *Oryza sativa*, and 14
342 PRONE-GEFs of *Arabidopsis thaliana*. Since the *O. sativa* PRONE-GEFs have not all been annotated so
343 far, we first constructed a maximum-likelihood phylogenetic tree via PhyML, in which all *O. sativa*
344 PRONE-GEFs were annotated according to their primary sequence similarity to *A. thaliana* PRONE-
345 GEFs using the nomenclature by Berken *et al.* (2005) (Fig. S1). Subsequently, another PhyML
346 calculation was performed to obtain the phylogenetic tree with all three species (Fig. 1). *H. vulgare*
347 PRONE-GEFs were then annotated according to the most closely related *O. sativa* PRONE-GEFs to
348 reach a nomenclature that is consistent for grasses. That way, the barley PRONE-GEFs were named
349 *Hv*GEFs 1, 2, 3a, 3b, 3c, 7, 9a, 9b, 9c, 10 and 14.
350 The resulting phylogenetic tree shows three distinct groups: clade (I), including PRONE-GEFs 1-7,
351 clade (II) clustering PRONE-GEFs 8-13 and a third clade consisting of only PRONE-GEF14 proteins from
352 the three different species (Fig. 1). Notably, in clades (I) and (II) we specifically found a clustering of
353 PRONE-GEFs from both monocot species and many high confidence branches with only *A. thaliana*
354 PRONE-GEFs suggesting PRONE-GEF gene duplications after the separation of monocots from dicots.
355 The three PRONE-GEF14 sequences differ not only in their variable N- and C- terminal regions from
356 the other PRONE-GEFs but present higher levels of amino acid changes in the PRONE domain itself
357 when compared to all other PRONE-GEFs (Fig. S1, Tab. S1). PRONE-GEF14 proteins are not present in
358 the moss *Physcomitrium patens* or the lycophyte *Selaginella moellendorffii* (Eklund *et al.*, 2010).
359 Despite its unique position in the phylogenetic tree, the overall structure of the *Hv*GEF14 PRONE
360 domain with its three sub-domains and essential amino acids for GEF-GEF and GEF-ROP interactions
361 is conserved when compared to the other barley PRONE-GEFs (Fig. 2).
362 The MUSCLE alignment of 11 barley PRONE-GEFs highlights the predicted PRONE domains (see Fig. 2)
363 with varying length of 344 amino acids (*Hv*GEF10) to 379 amino acids (*Hv*GEF3a) (Fig. S1, Tab. S2).

364 *Hv*GEF3a has no variable C-terminal region beyond the PRONE domain, and the C-terminus of
365 *Hv*GEF3b and *Hv*GEF3c are comparably short (Fig. 2, Fig. S1, Tab. S2). *Hv*GEF9a is predicted to contain
366 only a short variable N-terminus of 43 amino acids. It is evident from the alignment that, regarding
367 the primary sequence, *Hv*GEF14 substantially differs most from all other barley PRONE-GEFs. In
368 addition, the variability in primary sequence of *Hv*GEF14 is highest when compared to the consensus
369 sequence of all 11 *Hv*PRONE-GEFs (Fig. S1, Tab. S1). However, important residues for GEF-GEF
370 interaction (Thomas *et al.*, 2007) such as phenylalanine 133 and leucine 138 (in *Hv*GEF14) as well as
371 residues involved in GEF-ROP interaction N161, Q206, E215, M217, W275, W276, L434, and R460
372 (Thomas *et al.*, 2007) are conserved in *Hv*GEF14 (Fig. 2). Furthermore, *Hv*GEF14 full length and
373 PRONE domains only were shown to dimerise in Y2H (Fig. S3). Interestingly, serine 394 in the
374 *Hv*GEF14 PRONE domain, is a predicted phosphorylation site, based on mass spectrometry analysis of
375 phosphorylation sites in *A. thaliana* GEF14 (Mergner *et al.*, 2020). This putative phosphorylation site
376 is conserved in *At*GEF14 and *Hv*GEF14 but not outside the GEF14 clade.
377

378 **_Hv_GEF14 is expressed in epidermal cells and downregulated after _Bgh_ inoculation**

379 Based on their gene expression, *Arabidopsis* PRONE-GEFs have been shown to operate in different
380 plant tissues (Shin *et al.*, 2009; Zhang and McCormick, 2007). To understand the potential function of
381 barley *PRONE-GEF*s, gene expression patterns in different tissues were investigated. An initial *in silico*
382 expression analysis of the eight barley *PRONE-GEFs* was performed by consulting the RNAseq
383 database provided by The James-Hutton-Institute (https://ics.hutton.ac.uk/barleyGenes). In
384 accordance with previous studies in *A. thaliana*, the RNAseq data shows that some of the barley
385 *PRONE-GEF*s were expressed in distinct tissues only. *HvGEF3a*, for example, is mainly expressed in
386 the developing embryo. Other barley *GEFs*, like *HvGEF1*, show a broader expression pattern with
387 highest number of RNA fragments detected in embryos, root and grains. *HvGEF14* is the most
388 ubiquitously expressed PRONE-GEF of barley with highest fragment counts in almost all tissues,
389 except in senescing leaves. Interestingly, *HvGEF1* and *HvGEF14* are the only GEF genes expressed in

390 seedling shoots and epidermal peels with *HvGEF14* showing the highest fragment counts in these
391 two tissues compared to all other barley *PRONE-GEFs* (Tab. S6).
392 The leaf epidermis of barley provides an important interface for plant-pathogen interaction. Since
393 the barley type I ROP *Hv*RACB has been shown to play a crucial role in epidermis development and
394 susceptibility to the powdery mildew fungus (Schultheiss *et al.*, 2002), we concentrated on PRONE-
395 GEFs which might be of importance to signal transduction in the epidermis. We checked the gene
396 expression of *HvGEF14* via qRT-PCR in leaf and leaf epidermis from seven days old leaves of the
397 barley cultivar Golden Promise. In three independent biological replicates, we found higher transcript
398 levels of *HvGEF14* in the epidermis when compared to whole leaves (Fig. 3A). Notably, in three fully
399 independent biological experiments the *HvGEF14* expression level in the epidermis decreased after
400 inoculation with the biotrophic powdery mildew fungus *Bgh* compared to epidermal peels from
401 unchallenged leaves (Fig. 3B).
402
403 **_Hv_GEF14 interacts with _Hv_RACB**
404 *Hv*RACB is a barley ROP that supports fungal penetration by *Bgh* into epidermal cells, possibly by
405 supporting polar ingrowth of the fungal haustorium (Engelhardt *et al.*, 2020). So far, however,
406 nothing is known about a potential PRONE-GEF-mediated activation of *Hv*RACB. To check if *Hv*GEF14
407 is the putative HvRACB-activating PRONE-GEF, we analysed the direct protein-protein interaction
408 between *Hv*RACB and *Hv*GEF14 in yeast and *in planta*.
409 Plant ROPs can be mutagenized in the GTPase domain by exchanging a conserved glycine residue to
410 the hydrophobic valine (e.g., *Hv*RACB-G15V). These mutations render the ROP constitutively
411 activated (CA) regarding downstream signalling because of inactivating the intrinsic GTPase function,
412 which leads to a constantly GTP bound state (Schultheiss *et al.*, 2003). Correspondingly, the exchange
413 of a conserved threonine in the N-terminal part of the protein with asparagine keeps the ROP in a
414 dominant negative (DN) confirmation (*Hv*RACB-T20N). A third mutation (*Hv*RACB-D121N) can be
415 performed at an aspartic acid to an uncharged asparagine in order to lower nucleotide affinity and

416 potentially increase GEF-binding affinity (Akamatsu *et al.*, 2013; Berken *et al.*, 2005; Cool *et al.*,
417 1999).
418 Interestingly, we found that full length *Hv*GEF14 and the *Hv*GEF14 PRONE domain (amino acids 124-
419 485) directly interact in yeast with wild type *Hv*RACB, CA *Hv*RACB-G15V and the low nucleotide
420 affinity version *Hv*RACB-D121N, but not with the DN *Hv*RACB-T20N variant (Fig. 4). All *Hv*RACB
421 variants were truncated at the *Hv*RACB CSIL motif to inhibit prenylation and membrane association in
422 yeast and hence facilitate protein accumulation in yeast nuclei. To substantiate the results, we
423 performed Western Blots, which confirmed protein stability in yeast (Fig. S5).
424
425 To test direct protein-protein interaction between full-length *Hv*GEF14 and previously used variants
426 of *Hv*RACB *in planta*, we conducted a series of experiments measuring Förster resonance energy
427 transfer by fluorescence lifetime imaging (FRET- FLIM) in transiently transformed barley epidermal
428 cells. (Fig. 5). As a FRET fluorophore pair, monomeric enhanced green fluorescent protein (meGFP)
429 and red fluorescent protein mCherry were chosen for their proven effectiveness in plant protein-
430 protein interaction studies (Denay *et al.*, 2019). meGFP-*Hv*GEF14 served as FRET-donor and hence
431 was used unchanged as an interaction partner in every combination tested. As FRET acceptor,
432 different variants of mCherry-*Hv*RACB (WT, G15V, D121N, T20N) and free mCherry were used. All
433 measurements took place at the cell periphery at the equatorial cell plane and both fluorophores
434 were detected for the measurements in every case.
435 Using these donor/acceptor combinations, decreased meGFP-*Hv*GEF14 lifetime can be tested upon
436 co-expression with a particular mCherry-*Hv*RACB variant. In three repetitions, meGFP-*Hv*GEF14
437 lifetimes varied but showed a significant lifetime reduction in epidermal cells transiently co-
438 expressing meGFP-*Hv*GEF14 and mCherry-*Hv*RACB WT to 2.49 ns on average compared to the
439 negative control with free mCherry recorded at 2.64 ns. This suggests that *Hv*GEF14 interacts directly
440 with wild type *Hv*RACB *in planta* even though the fluorescence lifetime reduction varied in between
441 cells (Fig. 5). The transient co-expression of meGFP-*Hv*GEF14 with mCherry-CA *Hv*RACB-G15V also
442 resulted in a significantly reduced GFP-lifetime of 2.37 ns on average. This reflects the interaction

443 assays in yeast and provides further evidence that *Hv*GEF14 can also interact with the CA variant
444 *Hv*RACB-G15V *in planta* (Fig. 5). Similarly, co-expression of mCherry-fused *Hv*RACB-D121N mutant
445 significantly decreases the meGFP-*Hv*GEF14 lifetime to 2.57 ns on average. However, this
446 combination of proteins leads to a higher population of cells with meGFP-*Hv*GEF14 lifetimes similar
447 to control levels, demonstrating non-interacting proteins. However, these results confirmed the
448 direct interaction of *Hv*GEF14 with *Hv*RACB-D121N in yeast (Fig. 4). The only mCherry-tagged *Hv*RACB
449 variant, which did not provoke a reduced meGFP-*Hv*GEF14 lifetime when compared to the control,
450 was the DN *Hv*RACB-T20N mutant. As observed in yeast-two-hybrid assays, there was no measurable
451 interaction between *Hv*GEF14 and *Hv*RACB-T20N *in planta* (Fig. 5). In total, the FRET-FLIM
452 experiments suggest a direct interaction between *Hv*GEF14 full length and *Hv*RACB wild type, -G15V
453 and -D121N *in planta*.
454 To test for possible specificity of *Hv*GEF14-ROP interaction, we also tested the interaction with
455 *Hv*RAC1, another epidermis-expressed barley ROP that is of type II. In Y2H, *Hv*GEF14 interacted with
456 WT and the CA *Hv*RAC1-G23V but not with DN *Hv*RAC1-T28N (Fig. S6, S7).
457

458 **_Hv_GEF14 over expression leads to activation of barley ROPs**

459 Several ROP interacting proteins display a change of subcellular localisation in presence of an
460 activated ROP. This change in localisation is considered an indirect evidence for local ROP activity,
461 because those interactors preferable interact with GTP-loaded, signalling-activated ROPs (Li *et al.*,
462 2020; McCollum *et al.*, 2020; Schultheiss *et al.*, 2008). In transiently transformed epidermal cells, CA
463 *Hv*RACB is partially located at the cell periphery/plasma membrane, which depends on its C-terminal
464 CAAL prenylation motif (Schultheiss *et al.*, 2003; Schultheiss *et al.*, 2008). *Hv*RIC171, a barley scaffold
465 protein that has been shown to directly interact with CA but not DN barley ROP variants (Schultheiss
466 *et al.*, 2008), is recruited from the cytoplasm to the cell periphery and plasma membrane in the
467 presence of co-expressed CA *Hv*RACB-G15V but not DN *Hv*RACB-T20N. This strongly suggests *Hv*RACB
468 activation-dependent recruitment of *Hv*RIC171 (Schultheiss *et al.*, 2008). Based on this, we
469 monitored the localization of mCherry-tagged *Hv*RIC171 in barley epidermis cells in the presence or

470 absence of co-expressed *Hv*GEF14 to indirectly analyse the potential of *Hv*GEF14 to activate barley
471 ROPs like *Hv*RACB. mCherry-*Hv*RIC171 fluorescence significantly increased at the cell periphery when
472 *Hv*GEF14 was present compared to the empty vector (EV) control (Fig. 6A and B). This was evident
473 from an increase in normalised fluorescent signal intensity at the cell periphery in the equatorial
474 plane of the cell. Additionally, mCherry-*Hv*RIC171 signals appeared very irregular in the cell periphery
475 of control cells whereas mCherry-*Hv*RIC171 more evenly labelled the cell periphery of cells co-
476 expressing the putative ROP activator *Hv*GEF14 (Fig. 6A, lower panel).
477 To test specific activation of the susceptibility factor *Hv*RACB *in planta*, we made use of a FRET-based
478 activity sensor probe containing N-terminal meGFP-tagged *Hv*RACB and C-terminal mCherry-tagged
479 *Hv*CRIB46 on individual plasmids. Barley *Hv*CRIB46 represents an extended CRIB domain of HvRIC171
480 and was shown before to interact with CA *Hv*RACB but not DN *Hv*RACB. It can hence be considered,
481 such as CRIB domains in general, as preferably interacting with GTP-loaded RACB. To reduce
482 interference of endogenous signalling components in barley, the measurements were performed in
483 *N. benthamiana. meGFP-Hv*RACB WT did not interact with the negative control GST-mCherry (GFP
484 lifetime of 2.62 ns on average), but meGFP-*Hv*RACB WT lifetime is slightly but significantly reduced
485 when co-expressed with *Hv*CRIB46-mCherry (2.57 ns on average). This likely reflects the fact that wild
486 type HvRACB can switch between GDP and GTP loaded forms also in *N. benthamiana*. However,
487 when co-expressing HA-tagged *Hv*GEF14, we measured a significant decrease in meGFP fluorescence
488 lifetime, suggesting abundance of activated CRIB-binding *Hv*RACB-GTP. Since HA-*Hv*GEF14
489 transformation could not be verified in individual cells via microscopy, the protein was detected via
490 Western Blot after FRET-FLIM measurements (Fig. S8). As a positive control, the interaction of
491 meGFP-*Hv*RACB CA with *Hv*CRIB46-mCherry was measured at 2.35 ns on average (Fig. 7).
492

493 **_Hv_GEF14 supports barley susceptibility towards penetration by _Bgh_**

494 Since *HvGEF14* is expressed in barley shoot epidermis and interacts with two epidermis
495 expressed *Hv*ROPs, we tested the function of the exchange factor in the interaction of barley

496 and *Bgh*. Via transient single cell overexpression or RNAi-mediated silencing of *Hv*GEF14 in
497 barley epidermis cells and subsequent inoculation with fungal spores, we scored interaction
498 outcome for each transformed and attacked cell in at least five independent experiments.
499 On average we observed a significant increase of fungal success from 34.6% to 46.5%
500 penetration efficiency observed as haustorium formation in *Hv*GEF14 overexpressing cells
501 when compared to an empty vector control (Fig. 8).
502 We assessed the efficacy of RNAi-mediated gene silencing to 53% according to measuring
503 the reduction of GFP fluorescence intensities of single GFP-*Hv*GEF14 expressing barley cells
504 co-transformed with empty vector or *HvGEF14* gene silencing construct, respectively (Tab.
505 S7). The knock down of *HvGEF14* by RNAi led to the opposite effect of over-expression; a
506 decrease in penetration rate from 26.4% in the controls to only 16.5% in cells, in which
507 *HvGEF14* was silenced by RNAi. Absolute penetration rates are a bit lower in RNAi
508 experiments due to longer incubation time between microprojectile-mediated
509 transformation and inoculation and considerably varied from experiment to experiment
510 even in the controls. Accordingly, a p-value of 0.07 was computed during statistical analysis
511 of the means (Fig. 8). However, when comparing to individual controls, all six independent
512 repetitions of the experiment showed the same trend towards reduced penetration success
513 after knock-down of *HvGEF14*.

514 ## Discussion

515 The barley susceptibility factor *Hv*RACB has been studied over the last decades to
516 understand underlying molecular mechanisms of its role in support of fungal entry into
517 barley epidermal cells (Engelhardt *et al.*, 2020). However, a critical step in this pathway may
518 be the transition from a GDP-bound, signalling inactive, towards the GTP-loaded signalling
519 activated state of *Hv*RACB. As shown in the model species *A. thaliana* and in *O. sativa*, it is
520 apparent that plant specific PRONE-GEFs can facilitate the activation of ROP downstream
521 signalling. In this work, we therefore investigated the role of a barley PRONE-GEF candidate.
522 This revealed the epidermis-expressed and transcriptionally *Bgh*-regulated *Hv*GEF14 and its
523 likely role in ROP activation and susceptibility to fungal penetration.
524 According to our phylogenetic analysis, we suggest that PRONE-GEF14 has a unique position
525 in the evolution of PRONE-GEFs. A BLAST search with the primary sequence of *At*GEF14
526 reveals that the closest ortholog to PRONE-GEF14 in the moss *Physcomitrium patens* is
527 *Pp*GEF1 and that there is no PRONE-GEF14 found in the moss (see Eklund *et al.* (2010)). In
528 addition, in the liverwort *Marchantia polymorpha*, only one PRONE-GEF can be found in the
529 genome. The primary sequence of this PRONE-GEF, KARAPPO, is also most similar to *At*GEF1
530 (Fig. S8 and Hiwatashi *et al.* (2019). However, the ancient angiosperm species *Amborella*
531 seems to encode a GEF14 ortholog (protein accession XP_006878646). Hence, PRONE-GEF14
532 proteins might have evolved early in angiosperms before separation of monocots and dicots.
533 We could show the abundance of *HvGEF14* transcript in barley leaves and measured higher
534 transcript levels in epidermal peels when compared to whole leaves (Fig. 3A). Possible
535 candidate ROPs to interact with the gene product of *HvGEF14* in barley epidermis are the
536 five epidermis expressed small GTPases: *HvRACB*, *HvRAC1*, *HvRAC3*, *HvRACD* and *HvROP6*.
537 Furthermore, *HvRACB*, *HvRACD* and *HvROP6* had stronger transcript signals in the epidermis

538 compared to mesophyll in RT-PCR assays. When leaves were challenged with *Bgh*, several
539 susceptibility related barley ROP genes had slightly lower transcript levels compared to non-
540 inoculated controls (Schultheiss *et al.*, 2003). This gene expression profile in the epidermis is
541 reminiscent of the *HvGEF14* expression in barley epidermis during *Bgh* attack (Fig. 3B).
542 In the model plant *A. thaliana*, *AtGEF14* expression has also been reported in leaves via RT-
543 PCR experiments. In addition, *AtGEF14* expression patterns responded to a variety of abiotic
544 stresses (Shin *et al.*, 2009) which points to underlying regulatory mechanisms in response to
545 environmental signals. It is shown that a *Bgh* effector, *Bgh* ROP-interactive peptide 1, can
546 interact with *Hv*RACB and supports fungal virulence (Nottensteiner *et al.*, 2018). We
547 speculate that downregulation of *HvGEF14* transcripts and some barley *ROPs* could reflect a
548 plant response to fungal interference with host ROP signalling, to which the plant reacts by
549 countermeasures and downregulation of the susceptibility pathway. Alternatively,
550 downregulation of *HvGEF14* could reflect a re-allocation of resources from growth into
551 defence, if *Hv*GEF14 would have a physiological function in growth and development.
552 This study shows direct protein-protein interaction of *Hv*GEF14 with wild type *Hv*RACB, CA
553 *Hv*RACB-G15V and *Hv*RACB-D121N (low nucleotide affinity) (Fig. 4 and Fig. 5). In addition, we
554 report *Hv*GEF14 interaction with wild type *Hv*RAC1 and CA *Hv*RAC1-G23V in yeast (Fig. S6).
555 The fact that *Hv*GEF14 can interact with both, type I and type II ROPs suggests that it might
556 function in more than one signalling pathway. The interaction with WT ROPs provides the
557 basis for a possible role of this barley PRONE-GEF in small GTPase signalling.
558 In accordance with other studies in *A. thaliana*, which have previously shown interaction of
559 PRONE-GEFs with D121N-like low nucleotide affinity mutants of *At*ROPs (Akamatsu *et al.*,
560 2013; Berken *et al.*, 2005; Denninger *et al.*, 2019; Gu *et al.*, 2006), we could measure *in*
561 *planta* interaction of *Hv*RACB D121N with *Hv*GEF14. The initial discovery of the 14 *A.*

562 *thaliana* PRONE-GEFs was made in a yeast-two-hybrid screen with *At*ROP4 D121N as bait
563 (Berken *et al.*, 2005). A similar strategy was used to find PRONE-GEFs of *Os*RAC1 in *O. sativa*
564 (Akamatsu *et al.*, 2013). Furthermore, a global investigation into *At*GEF-*At*ROP1 interactions
565 showed that *At*GEF14 preferably interacts with a D121A/C188S mutant of *At*ROP1 *in vitro*
566 (Gu *et al.*, 2006). This interaction of PRONE-GEFs with low nucleotide affinity ROPs might
567 stem from the fact that these ROP mutants might still cycle between activated and
568 inactivated conformations while providing stronger affinity to PRONE-GEFs (Berken *et al.*,
569 2005). Alternatively, the D121N mutation might lead to a similar protein conformation as the
570 nucleotide free ROP, which has been crystallised in complex with the PRONE domain of
571 *At*GEF8 (Thomas *et al.*, 2007).
572 The interaction of PRONE-GEFs with other mutants of ROPs was also reported in *O. sativa*.
573 *Os*GEF1 interaction with *Os*RAC1 mutants was shown via split Venus fluorescence
574 complementation assays in protoplasts. Both, the constitutively activated *Os*RAC1-G19V as
575 well as the dominant negative *Os*RAC1-T24N variants were able to reconstitute fluorescence
576 of fluorescent Venus at the plasma membrane (Akamatsu *et al.*, 2013).
577 Interaction of PRONE-GEFs with CA ROPs has also been repeatedly reported here and before
578 (e.g., Akamatsu et al. 2013; Denninger et al. 2019). Together, data support that *Hv*GEF14 can
579 interact with *Hv*RACB in *planta*. Together with data from the literature, however, a picture
580 emerges that supports that PRONE-GEFs do not only interact with ROP-GDP but possibly can
581 stay in contact to ROP-GTP after nucleotide exchange. This could have several reasons,
582 which might be further studied. One possibility is that a PRONE-GEF-ROP(GTP) complex is
583 stabilised when the ROP is arrested in a CA status. Alternatively, activated ROPs might stay in
584 contact to GEFs for a feedback regulation on ROP activity through complexes formed with
585 ROP executers as discussed before (Wu and Lew, 2013). Because PRONE-GEFs including

586 *Hv*GEF14 can form dimers, GEF-GEF – ROP-GTP interaction could also recruit further ROP-
587 GDP for activation (Smokvarska *et al.*, 2021).
588 Sub-cellular localisation of signalling protein complexes is a key to ROP-mediated processes.
589 After activation, ROPs relocate to or are stabilized in their association with the plasma
590 membrane. There, they interact with downstream effectors/executers to facilitate, amongst
591 other functions, polar growth processes (Kawano *et al.*, 2014; Poraty-Gavra *et al.*, 2013;
592 Schultheiss *et al.*, 2003). During *A. thaliana* pollen tube growth, for example, the localisation
593 of activated *At*ROP1 to the apical plasma membrane regulates tip growth (Gu *et al.*, 2004).
594 This specific localisation of activated *At*ROP1 to the membrane leads to the accumulation of
595 downstream executers like *At*RIC4 in the same compartment. In presence of dominant
596 negative *At*ROP1, however, the RIC protein localises to the cytoplasm (Gu *et al.*, 2005). In
597 addition, the co-expression of a ROP-GAP, which renders *At*ROP1 inactive, also results in the
598 relocation of *At*RIC4 to the cytoplasm. In this model system of polar growth, the correct
599 localisation of activated *At*ROP1 as well as *At*RIC4 was observed to be crucial for
600 downstream signal transduction and fine tuning of the growth process (Hwang *et al.*, 2005).
601 To assess *Hv*RACB signalling activity status *in planta*, we made use of the previously
602 published recruitment of *Hv*RIC171 to CA *Hv*RACB-G15V, which otherwise largely resides at
603 the plasma membrane. In the same studies, *Hv*RIC171 was shown to be recruited to the site
604 of fungal penetration likely via endogenously activated ROPs (Schultheiss *et al.*, 2003;
605 Schultheiss *et al.*, 2008). Via confocal microscopy, we measured higher mCherry-*Hv*RIC171
606 localisation at the cell periphery in the presence of transiently over-expressed *Hv*GEF14 (Fig.
607 6). Based on previous work on *A. thaliana* and *H. vulgare* RICs, this finding suggests that the
608 over-expression of *Hv*GEF14 leads to a higher ratio of activated endogenous ROPs, which in
609 turn recruit *Hv*RIC171 towards the cell periphery. Another way to observe ROP activation *in*

610 *planta* is via CRIB-based ROP activity sensors that have previously been adapted for plants
611 (Kawano *et al.*, 2010; Wang *et al.*, 2018; Wong *et al.*, 2018). This so-called Ras and
612 interacting chimeric unit (Raichu) sensor includes the fluorophores Venus and CFP as FRET-
613 pair. ROP activity is monitored by its interaction with the CRIB domain of a downstream
614 executer. In a similar manner, we used the interaction of activated *Hv*RACB with a *Hv*RIC171
615 fragment containing the CRIB domain in FRET-FLIM assays using the efficient FRET-pair
616 meGFP and mCherry on separate plasmids (Denay *et al.*, 2019). With the setup in this study,
617 it is possible to monitor ROP activation status in *N. benthamiana* cells with different ROP and
618 interactor combinations. We observed a lower GFP-lifetime when we co-expressed
619 *Hv*GEF14, which strongly suggests that it can activate *Hv*RACB which leads to interaction of
620 GTP-loaded *Hv*RACB and *Hv*CRIB46 (Fig. 7).

621 In parallel, the transient over-expression of *Hv*GEF14 in barley epidermal cells leads to a
622 significant increase in *Bgh* penetration success (Fig. 8). This phenotype is similar to enhanced
623 fungal penetration during CA *Hv*RACB-G15V over-expression (Schultheiss *et al.*, 2003), as
624 well as the over-expression of *Hv*RACB-downstream executers, such as *Hv*RIC171
625 (Schultheiss *et al.*, 2008) and *Hv*RIPb (McCollum *et al.*, 2020). Transient silencing of *Hv*GEF14,
626 on the other hand, renders barley epidermis cells by trend more resistant to *Bgh* penetration
627 (Fig. 8). Even though the phenotype could be observed in every repetition when comparing
628 *Hv*GEF14 RNAi with its respective control, the extend of fungal penetration varied amongst
629 repetitions so that the significance threshold of 0.05 was not met after statistical analysis.
630 Considering however, that the inoculation with *Bgh* naturally decreases the transcript of
631 *HvGEF14* (see Fig. 3), additional ectopic knock down perhaps cannot be expected to exert a
632 major additional effect. Taken together, these assays point to a role of *Hv*GEF14 in
633 supporting the accommodation of *Bgh* infection structures in barley epidermal cells, similar

634 to and possibly in cooperation with the susceptibility factor *Hv*RACB and other epidermis
635 expressed *Hv*ROPs (Schultheiss *et al.*, 2003).

636 An overview and comprehensive annotation of the PRONE-GEFs from *A. thaliana*, *O. sativa*
637 and *H. vulgare* was prepared using maximum likelihood phylogenetic analysis. The analysed
638 PRONE-GEFs distribute into three clades based on high bootstrap values at the branching
639 points (Fig. 1) which is partly in accordance with previously published PRONE-GEF
640 phylogenies (Berken *et al.*, 2005; Kim *et al.*, 2020; Shin *et al.*, 2009; Zhang and McCormick,
641 2007). Shin and colleagues (2009) use the same alignment algorithm as in this study to build
642 a dendrogram of *A. thaliana* PRONE-GEFs. The resulting tree does not include bootstrap
643 analysis but also highlights three clades of PRONE-GEFs with different distribution when
644 compared to the clades published in this study. In their analysis, *At*GEF14 belongs to group
645 2, and *At*GEF1 is most separated from all other *A. thaliana* PRONE-GEFs (Shin *et al.*, 2009).
646 Our results, however, indicate that PRONE-GEF1 from all three species cluster in clade I (Fig.
647 1). *At*GEF14 is placed next to *At*GEF12 and *At*GEF11 in Shin et al. (2009). This is also the case
648 in Berken *et al.* (2005) who report a phylogram of *A. thaliana*, *O. sativa*, *M. truncatula* (*Mt*)
649 and *L. esculentum* (*Le*) PRONE-GEFs. The resulting TreeView phylogeny in Berken *et al.*
650 (2005) also does not report bootstrap values and differs to our phylogenetic tree in the early
651 branching of *At*GEF7. Another phylogeny has been published by Zhang and McCormick
652 (2007) who compare to that date known PRONE-GEFs from *A. thaliana*, *O. sativa*, *P. patens*
653 (*Pp*), *M. truncatula* (*Mt*) and *L. esculentum* (*Le*). Based on CLUSTALW alignment and
654 MEGA3.1 neighbour joining algorithm with bootstrap analysis, the authors define two
655 distinct groups of PRONE-GEFs with *At*GEFs 8, 9, 11, 12, 13 and 14 as well as *Le*KPP and
656 *Mt*GEF1 in one group with several non-annotated *Os*GEFs. In addition to the two groups of
657 PRONE-GEFs published by Zhang and McCormick (2007), we emphasize the branching of

658 PRONE-GEF14 proteins (with high confidence of bootstrap value 100) by dividing previously
659 published clade II further and highlighting the unique position of PRONE-GEF14 in a separate
660 clade III. A more recently published PRONE-GEF alignment compares *A. thaliana* and *O.*
661 *sativa* proteins (Kim *et al.*, 2020) with similar methods as has been used here. Though the
662 annotation of *Os*GEFs does not match with previously published *Os*GEF nomenclature we
663 can confirm distinct clades of PRONE-GEFs 1-7 and 8-13 as well as the placement of PRONE-
664 GEF14 separated from the other two clades (Fig. 1 and (Kim *et al.*, 2020)). Due to high
665 confidence bootstrap analysis and comprehensive annotation of *O. sativa* and *H. vulgare*
666 PRONE-GEFs, we propose to base further comparisons on the presented phylogeny (Fig. 1). A
667 unique position of GEF14 proteins in the phylogeny of PRONE-GEFs is further supported by
668 its comparably low sequence conservation of the PRONE domain, when compared to all
669 other PRONE-GEFs (Fig. S1, Tab. S1).

670 In conclusion, *Hv*GEF14 is a *bona fide* barley PRONE-GEF and interacts with barley ROPs. The
671 interaction with susceptibility-related barley ROPs might lead to ROP activation and
672 therefore facilitate ROP functions in susceptibility to invasion by *Bgh*. Research on *A.*
673 *thaliana* PRONE-GEFs highlights the interplay of different PRONE-GEFs to facilitate polar
674 growth processes like root hair formation or pollen tube growth (Denninger *et al.*, 2019; Li *et*
675 *al.*, 2020). It has to be studied if *Hv*GEF14 function is choreographed in a similar manner with
676 other barley PRONE-GEFs. In addition, other PRONE-GEF interactors, such as potential
677 upstream RLKs, remain to be investigated. In future studies, susceptibility- and *Hv*RACB-
678 related candidate RLKs (Douchkov *et al.*, 2014; Schnepf *et al.*, 2018) will be of special interest
679 to link *Hv*RACB signalling to cell surface signal perception.
680

681 ## Supplementary data

682 Fig. S1: Phylogenetic tree of *A. thaliana* and *O. sativa* PRONE-GEFs.

683 Fig. S2: MUSCLE alignment of *A. thaliana*, *O. sativa* and *H. vulgare* PRONE-GEFs.

684 Fig. S3: *Hv*GEF14 homo-dimerises with full length and PRONE domain (amino acids 124-485) in yeast-
685 two hybrid.

686 Fig. S4: Original images of *Hv*GEF14 full length and PRONE domain (amino acids 124-485) interaction
687 with *Hv*RACB variants (wild type, WT; G15V; D121N; T20N) via yeast-two hybrid.

688 Fig. S5: Western Blot of yeast proteins of Y2H *Hv*GEF14 interaction with *Hv*RACB on PVDF
689 membranes.

690 Fig. S6: *Hv*RAC1 wild type (WT), G23V constitutively activated (CA), T28N dominant negative (DN)
691 variants were tested as bait against prey constructs *Hv*GEF14 full length, *Hv*GEF14 124-485 (PRONE
692 domain) or empty vector (EV).

693 Fig. S7: Western Blot of yeast proteins Y2H *Hv*GEF14 interaction with *Hv*RAC1 on PVDF membranes.

694 Fig. S8: Western Blot of proteins extracted from *N. benthamiana* on PVDF membranes.

695 Table S1: Primary sequence similarity of HvGEFs when compared to consensus sequence shows
696 highest variability of HvGEF14 primary sequence.

697 Table S2: List of barley PRONE-GEFs with gene/protein identifiers, annotation, PRONE prediction, and
698 protein sequence length.

699 Table S3: List of plasmids used in this study.

700 Table S4: List of primers used in this study.

701 Table S6: Tissue-specific *Hv*GEF gene expression based on RNAseq (James Hutton Institute) in
702 fragments per reads per kilobase million (FPKM).

703 Table S7: RNAi efficiency of GEF14 hairpin construct in transient transformation of barley epidermal
704 cells.

705

706

Acknowledgements

We would like to acknowledge Johanna Hofer for outstanding technical assistance as well as Carolina Galgenmüller. Thanks goes to Parvinderdeep Kahlon and Lina Muñoz for critical reading of the manuscript as well as Lukas Weiss, Christopher McCollum and Michaela Stegmann for intellectual input and methodological assistance. We would like to thank the Center of Advanced Light Microscopy (CALM) imaging centre of TUM for providing access to the FRET-FLIM system. We are grateful to the German Research Foundation (DFG) for funding this work via SFB924.

Author contributions

RH was responsible for conception and AT, SE and RH designed the work. Data acquisition and analysis was performed by AT as well as interpretation of the data in collaboration with SE and RH. SE assisted in data acquisition for Fig. 8. AT drafted the manuscript and prepared the final version of the work after revision by SE and RH. All authors have approved the submitted version and have agreed both to be personally accountable for the author's own contributions and to ensure that questions related to the accuracy or integrity of any part of the work, even ones in which the author was not personally involved, are appropriately investigated, resolved, and the resolution documented in the literature.

Data availability statement

All data generated or analysed during this study are included in this published article [and its supplementary information files]. Additional datasets used and/or analysed during the current study are available from the corresponding author on reasonable request.

References

Akamatsu A, Uno K, Kato M, Wong HL, Shimamoto K, Kawano Y. 2015. New insights into the dimerization of small GTPase Rac/ROP guanine nucleotide exchange factors in rice. Plant signaling and behavior **10**, e1044702.

Akamatsu A, Wong HL, Fujiwara M, Okuda J, Nishide K, Uno K, Imai K, Umemura K, Kawasaki T, Kawano Y, Shimamoto K. 2013. An OsCEBiP/OsCERK1-OsRacGEF1-OsRac1 module is an essential early component of chitin-induced rice immunity. Cell host & microbe **13**, 465–476.

Berken A, Thomas C, Wittinghofer A. 2005. A new family of RhoGEFs activates the Rop molecular switch in plants. Nature **436**, 1176–1180.

Bloch D, Yalovsky S. 2013. Cell polarity signaling. Current opinion in plant biology **16**, 734–742.

Chang F, Gu Y, Ma H, Yang Z. 2013. AtPRK2 promotes ROP1 activation via RopGEFs in the control of polarized pollen tube growth. Molecular plant **6**, 1187–1201.

Chen M, Liu H, Kong J, Yang Y, Zhang N, Li R, Yue J, Huang J, Li C, Cheung AY, Tao L-Z. 2011. RopGEF7 Regulates PLETHORA-Dependent Maintenance of the Root Stem Cell Niche in Arabidopsis. The Plant cell **23**, 2880-2894.

Chen X, Friml J. 2014. Rho-GTPase-regulated vesicle trafficking in plant cell polarity. Biochemical Society transactions **42**, 212–218.

Chomczynski P, Sachhi N. 1987. Single-step Method of RNA Isolation by Acid Guanidinium Thiocyanate-Phenol-Chloroform Extraction. Analytical Biochemistry **162**, 156-159.

Cool RH, Schmidt G, Lenzen CU, Prinz H, Vogt D, Wittinghofer A. 1999. The Ras Mutant D119N Is Both Dominant Negative and Activated. MOLECULAR AND CELLULAR BIOLOGY **19**, 6297–6305.

Denay G, Schultz P, Hansch S, Weidtkamp-Peters S, Simon R. 2019. Over the rainbow: A practical guide for fluorescent protein selection in plant FRET experiments. Plant Direct **3**, 1–14.

Denninger P, Reichelt A, Schmidt VAF, Mehlhorn DG, Asseck LY, Stanley CE, Keinath NF, Evers JF, Grefen C, Grossmann G. 2019. Distinct RopGEFs Successively Drive Polarization and Outgrowth of Root Hairs. Current Biology **29**, 1854-1865 e1855.

Douchkov D, Lück S, Johrde A, Nowara D, Himmelbach A, Rajaraman J, Stein N, Sharma R, Kilian B, Schweizer P. 2014. Discovery of genes affecting resistance of barley to adapted and non-adapted powdery mildew fungi. Genome Biology **15**.

Eklund DM, Svensson EM, Kost B. 2010. Physcomitrella patens: a model to investigate the role of RAC/ROP GTPase signalling in tip growth. Journal of experimental botany **61**, 1917–1937.

Engelhardt S, Trutzenberg A, Hueckelhoven R. 2020. Regulation and Functions of ROP GTPases in Plant-Microbe Interactions. Cells **9**.

Fehér A, Lajkó DB. 2015. Signals fly when kinases meet Rho-of-plants (ROP) small G-proteins. Plant Science **237**, 93–107.

Gu Y, Fu Y, Dowd P, Li S, Vernoud V, Gilroy S, Yang Z. 2005. A Rho family GTPase controls actin dynamics and tip growth via two counteracting downstream pathways in pollen tubes. Journal of Cell Biology **169**, 127-138.

Gu Y, Li S, Lord EM, Yang Z. 2006. Members of a novel class of Arabidopsis Rho guanine nucleotide exchange factors control Rho GTPase-dependent polar growth. The Plant cell **18**, 366–381.

Gu Y, Wang Z, Yang Z. 2004. ROP/RAC GTPase: An old new master regulator for plant signaling. Current opinion in plant biology **7**, 527–536.

Hiwatashi T, Goh H, Yasui Y, Koh LQ, Takami H, Kajikawa M, Kirita H, Kanazawa T, Minamino N, Togawa T, Sato M, Wakazaki M, Yamaguchi K, Shigenobu S, Fukaki H, Mimura T, Toyooka K, Sawa S, Yamato KT, Ueda T, Urano D, Kohchi T, Ishizaki K. 2019. The RopGEF KARAPPO Is Essential for the Initiation of Vegetative Reproduction in Marchantia polymorpha. Current Biology **29**, 1-7.

Hoefle C, Huesmann C, Schultheiss H, Börnke F, Hensel G, Kumlehn J, Hückelhoven R. 2011. A barley ROP GTPase ACTIVATING PROTEIN associates with microtubules and regulates entry of the barley powdery mildew fungus into leaf epidermal cells. The Plant cell **23**, 2422–2439.

Hoefle C, McCollum C, Hückelhoven R. 2020. Barley ROP-Interactive Partner-a organizes into RAC1- and MICROTUBULE-ASSOCIATED ROP-GTPASE ACTIVATING PROTEIN 1-dependent membrane domains. BMC Plant Biology **20**, 1-12.

Huang C, jiao X, Yang L, Zhang M, Dai M, Wang L, Wang K, Bai L, Song C. 2018a. ROP-GEF signal transduction is involved in AtCAP1-regulated root hair growth. Plant Growth Regulation **87**, 1-8.
Huang J, Liu H, Berberich T, Liu Y, Tao LZ, Liu T. 2018b. Guanine Nucleotide Exchange Factor 7B (RopGEF7B) is involved in floral organ development in Oryza sativa. Rice (N Y) **11**, 1-13.
Hückelhoven R, Dechert C, Kogel KH. 2003. Overexpression of barley BAX inhibitor 1 induces breakdown of mlo-mediated penetration resistance to Blumeria graminis. Proceedings of National Academy of Science USA **100**, 5555-5560.
Hwang J-U, Gu Y, Lee Y-J, Yang Z. 2005. Oscillatory ROP GTPase Activation Leads the Oscillatory Polarized Growth of Pollen Tubes. Molecular Biology of the Cell **16**, 5385–5399.
International Barley Genome Sequencing Consortium T. 2012. A physical, genetic and functional sequence assembly of the barley genome. Nature **491**, 711-715.
Kawano Y, Akamatsu A, Hayashi K, Housen Y, Okuda J, Yao A, Nakashima A, Takahashi H, Yoshida H, Wong HL, Kawasaki T, Shimamoto K. 2010. Activation of a Rac GTPase by the NLR family disease resistance protein Pit plays a critical role in rice innate immunity. Cell Host Microbe **7**, 362-375.
Kawano Y, Kaneko-Kawano T, Shimamoto K. 2014. Rho family GTPase-dependent immunity in plants and animals. Frontiers in plant science **5**, 522.
Kim E-J, Park S-W, Hong W-J, Silva J, Liang W, Zhang D, Jung K-H, Kim Y-J. 2020. Genome-wide analysis of RopGEF gene family to identify genes contributing to pollen tube growth in rice (Oryza sativa). BMC Plant Biology **20**, 1.
Li E, Zhang YL, Shi X, Li H, Yuan X, Li S, Zhang Y. 2020. A positive feedback circuit for ROP-mediated polar growth. Molecular plant **14**, 395-410.
Lin W, Tang W, Anderson C, Yang Z. 2018. FERONIA's sensing of cell wall pectin activates ROP GTPase signaling in Arabidopsis. BioRxiV, 33.
Liu J, Liu MX, Qiu LP, Xie F. 2020. SPIKE1 Activates the GTPase ROP6 to Guide the Polarized Growth of Infection Threads in Lotus japonicus. Plant Cell **32**, 3774-3791.
Livak KJ, Schmittgen TD. 2001. Analysis of relative gene expression data using real-time quantitative PCR and the 2(-Delta Delta C(T)) Method. Methods **25**, 402–408.
Mascher M, Wicker T, Jenkins J, Plott C, Lux T, Koh CS, Ens J, Gundlach H, Boston LB, Tulpova Z, Holden S, Hernandez-Pinzon I, Scholz U, Mayer KFX, Spannagl M, Pozniak CJ, Sharpe AG, Simkova H, Moscou MJ, Grimwood J, Schmutz J, Stein N. 2021. Long-read sequence assembly: a technical evaluation in barley. Plant Cell **0**, 1-19.
McCollum C, Engelhardt S, Weiss L, Huckelhoven R. 2020. ROP INTERACTIVE PARTNER b Interacts with RACB and Supports Fungal Penetration into Barley Epidermal Cells. Plant Physiol **184**, 823-836.
Mergner J, Frejno M, List M, Papacek M, Chen X, Chaudhary A, Samaras P, Richter S, Shikata H, Messerer M, Lang D, Altmann S, Cyprys P, Zolg DP, Mathieson T, Bantscheff M, Hazarika RR, Schmidt T, Dawid C, Dunkel A, Hofmann T, Sprunck S, Falter-Braun P, Johannes F, Mayer KFX, Jurgens G, Wilhelm M, Baumbach J, Grill E, Schneitz K, Schwechheimer C, Kuster B. 2020. Mass-spectrometry-based draft of the Arabidopsis proteome. Nature **579**, 409-414.
Mucha E, Fricke I, Schaefer A, Wittinghofer A, Berken A. 2011. Rho proteins of plants--functional cycle and regulation of cytoskeletal dynamics. European Journal of Cell Biology **90**, 934-943.
Nagawa S, Xu T, Yang Z. 2010. RHO GTPase in plants: Conservation and invention of regulators and effectors. Small GTPases **1**, 78–88.
Nibau C, Wu HM, Cheung AY. 2006. RAC/ROP GTPases: 'hubs' for signal integration and diversification in plants. Trends Plant Science **11**, 309-315.
Nottensteiner M, Zechmann B, McCollum C, Huckelhoven R. 2018. A Barley Powdery Mildew Fungus Non-Autonomous Retrotransposon Encodes a Peptide that Supports Penetration Success on Barley. Journal of experimental botany **69**, 293745–293758.
Opalski KS, Schultheiss H, Kogel K-H, Hückelhoven R. 2005. The receptor-like MLO protein and the RAC/ROP family G-protein RACB modulate actin reorganization in barley attacked by the biotrophic powdery mildew fungus Blumeria graminis f.sp. hordei. The Plant journal : for cell and molecular biology **41**, 291–303.

Pathuri IP, Zellerhoff N, Schaffrath U, Hensel G, Kumlehn J, Kogel K-H, Eichmann R, Hückelhoven R. 2008. Constitutively activated barley ROPs modulate epidermal cell size, defense reactions and interactions with fungal leaf pathogens. Plant cell reports **27**, 1877–1887.
Poraty-Gavra L, Zimmermann P, Haigis S, Bednarek P, Hazak O, Stelmakh OR, Sadot E, Schulze-Lefert P, Gruissem W, Yalovsky S. 2013. The Arabidopsis Rho of plants GTPase AtROP6 functions in developmental and pathogen response pathways. Plant Physiology **161**, 1172–1188.
Qiu JL, Jilk R, Marks MD, Szymanski DB. 2002. The Arabidopsis SPIKE1 gene is required for normal cell shape control and tissue development. Plant Cell **14**, 101-118.
Qu S, Zhang X, Song Y, Lin J, Shan X. 2017. THESEUS1 positively modulates plant defense responses against Botrytis cinerea through GUANINE EXCHANGE FACTOR4 signaling. Journal of Integrative Plant Biology **59**, 797–804.
Scheler B, Schnepf V, Galgenmüller C, Ranf S, Hückelhoven R. 2016. Barley disease susceptibility factor RACB acts in epidermal cell polarity and positioning of the nucleus. Journal of experimental botany **67**, 3263–3275.
Schmidt A, Hall A. 2002. Guanine nucleotide exchange factors for Rho GTPases: turning on the switch. Genes & Development **16**, 1587–1609.
Schnepf V, Vlot AC, Kugler K, Hückelhoven R. 2018. Barley susceptibility factor RACB modulates transcript levels of signalling protein genes in compatible interaction with Blumeria graminis f.sp. hordei. Molecular plant pathology **19**, 393–404.
Schultheiss H, Dechert C, Kogel K-H, Hückelhoven R. 2002. A small GTP-binding host protein is required for entry of powdery mildew fungus into epidermal cells of barley. Plant Physiology **128**, 1447–1454.
Schultheiss H, Dechert C, Kogel K-H, Hückelhoven R. 2003. Functional analysis of barley RAC/ROP G-protein family members in susceptibility to the powdery mildew fungus. The Plant Journal **36**, 589–601.
Schultheiss H, Hensel G, Imani J, Broeders S, Sonnewald U, Kogel K-H, Kumlehn J, Hückelhoven R. 2005. Ectopic expression of constitutively activated RACB in barley enhances susceptibility to powdery mildew and abiotic stress. Plant Physiology **139**, 353–362.
Schultheiss H, Preuss J, Pircher T, Eichmann R, Hückelhoven R. 2008. Barley RIC171 interacts with RACB in planta and supports entry of the powdery mildew fungus. Cellular microbiology **10**, 1815–1826.
Shin DH, Kim T-L, Kwon Y-K, Cho M-H, Yoo J, Jeon J-S, Hahn T-R, Bhoo SH. 2009. Characterization of Arabidopsis RopGEF family genes in response to abiotic stresses. Plant Biotechnology Reports **3**, 183-190.
Smokvarska M, Jaillais Y, Martiniere A. 2021. Function of membrane domains in Rho-Of-Plant signaling. Plant Physiology **185**, 663–681.
Tang W, Lin W, Li B, Yang Z. 2021. Mechano-transduction via the pectin-FERONIA complex regulates ROP6 GTPase signaling in Arabidopsis. BioRxiV.
Thomas C, Fricke I, Scrima A, Berken A, Wittinghofer A. 2007. Structural evidence for a common intermediate in small G protein-GEF reactions. Molecular cell **25**, 141–149.
Thomas C, Fricke I, Weyand M, Berken A. 2009. 3D structure of a binary ROP-PRONE complex: The final intermediate for a complete set of molecular snapshots of the RopGEF reaction. Biological chemistry **390**, 427–435.
Vetter IR, Wittinghofer A. 2001. The guanine nucleotide-binding switch in three dimensions. Science **294**, 1299-1304.
Wang Q, Li Y, Ishikawa K, Kosami K-I, Uno K, Nagawa S, Tan L, Du J, Shimamoto K, Kawano Y. 2018. Resistance protein Pit interacts with the GEF OsSPK1 to activate OsRac1 and trigger rice immunity. Proceedings of the National Academy of Sciences of the United States of America **115**, 1-10.
Winge P, Brembu T, Kristensen R, Bones AM. 2000. Genetic Structure and Evolution of RAC-GTPases in Arabidopsis thaliana. Genetics **156**, 1959-1971.
Wong HL, Akamatsu A, Wang Q, Higuchi M, Matsuda T, Okuda J, Kosami KI, Inada N, Kawasaki T, Kaneko-Kawano T, Nagawa S, Tan L, Kawano Y, Shimamoto K. 2018. In vivo monitoring of plant small GTPase activation using a Forster resonance energy transfer biosensor. Plant Methods **14**, 56.

Wu C-F, Lew DJ. 2013. Beyond symmetry-breaking: Competition and negative feedback in GTPase regulation. Trends in cell biology **23**, 476–483.
Wu G, Li H, Yang Z. 2000. Arabidopsis RopGAPs Are a Novel Family of Rho GTPase-Activating Proteins that Require the Cdc42/Rac- Interactive Binding Motif for Rop-Specific GTPase Stimulation. Plant Physiology **124**, 1625-1636.
Yalovsky S. 2015. Protein lipid modifications and the regulation of ROP GTPase function. Journal of experimental botany **66**, 1617-1624.
Yamaguchi K, Imai K, Akamatsu A, Mihashi M, Hayashi N, Shimamoto K, Kawasaki T. 2012. SWAP70 functions as a Rac/Rop guanine nucleotide-exchange factor in rice. The Plant Journal **70**, 389–397.
Yamaguchi K, Kawasaki T. 2012. Function of Arabidopsis SWAP70 GEF in immune response. Plant signaling & behavior **7**, 465–468.
Yang Y, Li R, Qi M. 2000. In vivo analysis of plant promoters and transcription factors by agroinfiltration of tobacco leaves. The Plant Journal **22**, 543-551.
Yoo JH, Park J-H, Cho S-H, Yoo S-C, Li J, Zhang H, Kim K-S, Koh H-J, Paek N-C. 2011. The rice bright green leaf (bgl) locus encodes OsRopGEF10, which activates the development of small cuticular papillae on leaf surfaces. Plant molecular biology **77**, 631–641.
Zhang T, Lei J, Yang H, Xu K, Wang R, Zhang Z. 2011. An improved method for whole protein extraction from yeast Saccharomyces cerevisiae. Yeast **28**, 795-798.
Zhang Y, McCormick S. 2007. A distinct mechanism regulating a pollen-specific guanine nucleotide exchange factor for the small GTPase Rop in Arabidopsis thaliana. Proceedings of the National Academy of Sciences of the United States of America **104**, 18830–18835.
Zheng Z-L, Yang Z. 2000. The Rop GTPase: an emerging switch in plants. Plant molecular biology, 1-9.

Figure Legends

Fig.1: **PRONE-GEFs cluster in three distinctive clades**. Phylogenetic analysis of PRONE-GEFs of

Arabidopsis thaliana (*At*), *Oryza sativa* (*Os*) and *Hordeum vulgare* (*Hv*) based on MUSCLE alignment.

Maximum likelihood tree was calculated based on available amino acid sequences (NCBI and barley Morex genome version3) and annotation of barley PRONE-GEFs was performed based on this tree.

Fig.2: ***Hordeum vulgare* (*Hv*) PRONE-GEF** MUSCLE alignment with annotation of PRONE domain (according to NCBI prediction) in grey, GEF-GEF interaction residues and ROP-GEF interaction residues highlighted in purple. Predicted phosphorylation site in *Hv*GEF14 highlighted in turquoise. Protein IDs according to NCBI accessions and annotation based on MUSCLE alignment with *O. sativa* PRONE-GEFs (see Fig. S1)

Fig. 3: ***HvGEF14* shows increased expression in epidermal peels and downregulation after inoculation with fungal spores.** *HvGEF14* is expressed in barley epidermis (A) and downregulated after Bgh inoculation (1 dpi) (B) in three independent repetitions (plants harvested on different days). Foldchange expression was calculated with primer efficiency correction and the 2^(-ddCt) method by Livak and Schmittgen (2001) and normalised to transcript levels in whole leaves (A) and non- inoculated epidermis (B).

Fig.4: ***Hv*GEF14 interacts with barley ROP variants in yeast**. *Hv*RACB wild type (WT), G15V constitutively activated (CA), T20N dominant negative (DN) and D121N low nucleotide affinity variants were tested as bait against prey constructs *Hv*GEF14 full length, *Hv*GEF14 amino acids 124-485 (PRONE domain) or empty vector (EV). Interaction of proteins shown on media containing amino acid mix without leucine (L), tryptophan (W) and histidine (H), (-L-W-H) in two dilutions (factor 10^{-1}) to identify growth of single yeast colonies. Representative image of three experiments with the same result. Successful yeast transformation was confirmed with selective media (amino acid mix without leucine (L) and tryptophan (W) (-L-W). Dropout was performed on one -L-W and one -L-W-H plate and images were cropped during figure preparation for better visibility. Original images can be found in Fig. S1 (Fig. S4).

Fig. 5: ***Hv*GEF14 interacts with HvRACB variants in planta**. GFP-tagged *Hv*GEF14 full length was observed in FRET-FLIM experiments to interact with mCherry-tagged *Hv*RACB wild type (WT), constitutively activated (G15V) and low nucleotide affinity mutant (D121N) but not with dominant negative (T20N) RACB. Mean GFP lifetime is indicated with black point, n = number of cells observed in three independent experiments. Mean shown as orange dot. Kruskal-Wallis p-value = 4.346e-14, pairwise comparison was performed via wilcoxon test and bonferroni adjustment for multiple testing. (Rstudio, version 1.2.5033).

Fig. 6: ***Hv*GEF14 influences subcellular localisation of mCherry-*Hv*RIC171**. Localisation of mCherry-*Hv*RIC171, a downstream interactor of activated ROPs in barley, shows higher fluorescence intensity at the cell periphery when *Hv*GEF14 is co-expressed simultaneously. (A) Representative images of three biological replicates show z-stack and equatorial plane of mCherry-*Hv*RIC171 and cytosolic GFP fluorescence of transiently transformed barley epidermis cells. (B) Quantification of periphery mCherry fluorescence intensity normalized to whole cell mCherry and GFP fluorescence intensity measured in minimum 30 cells via Fiji, statistical analysis performed in Rstudio via wilcox test (Rstudio *version 1.2.5033*).

Fig. 7: ***Hv*RACB can be activated by *Hv*GEF14.** meGFP-*Hv*RACB interacts with *Hv*CRIB46-mCherry, a 46 amino acid fragment of *Hv*RIC171, when mutated (G15V) to a constitutively activated variant or in presence of *Hv*GEF14 during FRET-FLIM measurements in *N. benthamiana*. GST-mCherry used as negative control. Summary of six independent repetitions, Kruskal-Wallis comparison of means performed in Rstudio (version 1.2.5033) after testing for distribution of data.

Fig. 8: ***Hv*GEF14 affects *Bgh* penetration efficiency.** *Bgh* penetration efficiency in barley epidermis cells over-expressing (OE) *Hv*GEF14 full length compared to mean penetration

efficiency in cells with pGY1 empty vector (control OE) or after knock-down (KD) of *HvGEF14* via RNAi compared to mean penetration efficiency of pIPKTA30N empty vector (control KD). Mean values indicated with bar. Statistical significance of differences of the mean calculated with t-test in Rstudio (version 1.2.5033) after assessing for normal distribution with Shapiro-Wilk test.

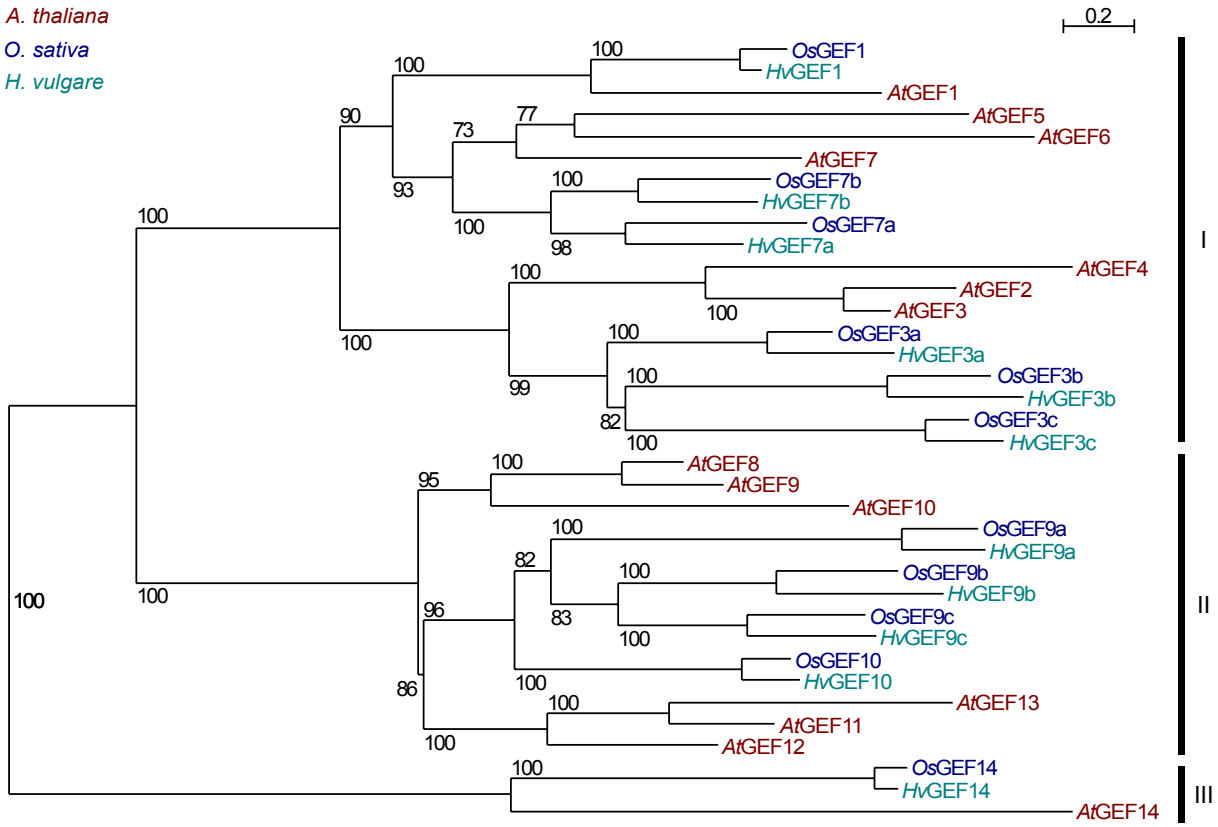

Fig.1: **PRONE-GEFs cluster in three distinctive clades**. Phylogenetic analysis of PRONE-GEFs of *Arabidopsis thaliana* (*At*), *Oryza sativa* (*Os*) and *Hordeum vulgare* (*Hv*) based on MUSCLE alignment. Maximum likelihood tree was calculated based on available amino acid sequences (NCBI and barley Morex genome version3) and annotation of barley PRONE-GEFs was performed based on this tree.

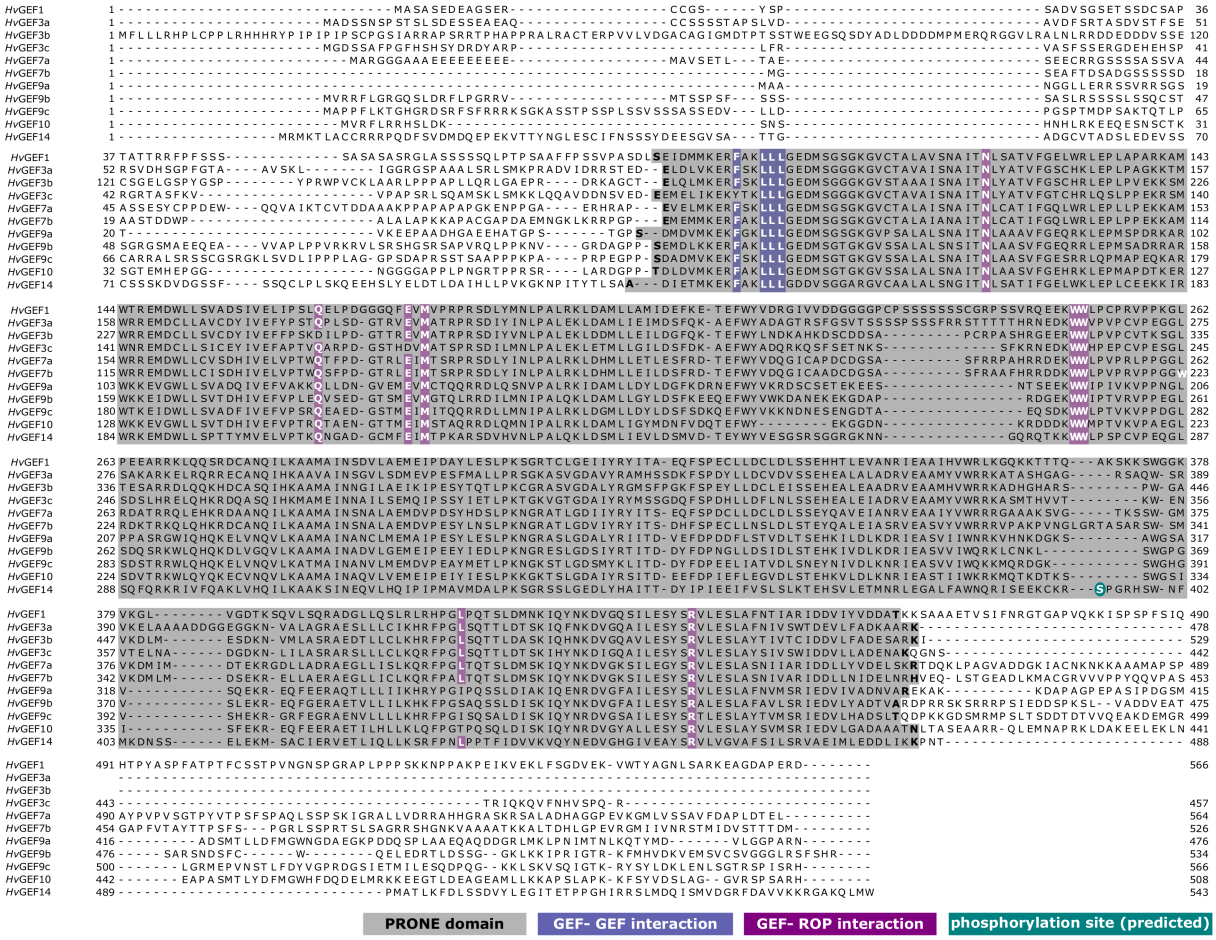

Fig.2: ***Hordeum vulgare* (*Hv*) PRONE-GEF** MUSCLE alignment with annotation of PRONE domain (according to NCBI prediction) in grey, GEF-GEF interaction residues and ROP-GEF interaction residues highlighted in purple. Predicted phosphorylation site in *Hv*GEF14 highlighted in turquoise. Protein IDs according to NCBI accessions and annotation based on MUSCLE alignment with *O. sativa* PRONE-GEFs (see Fig. S1)

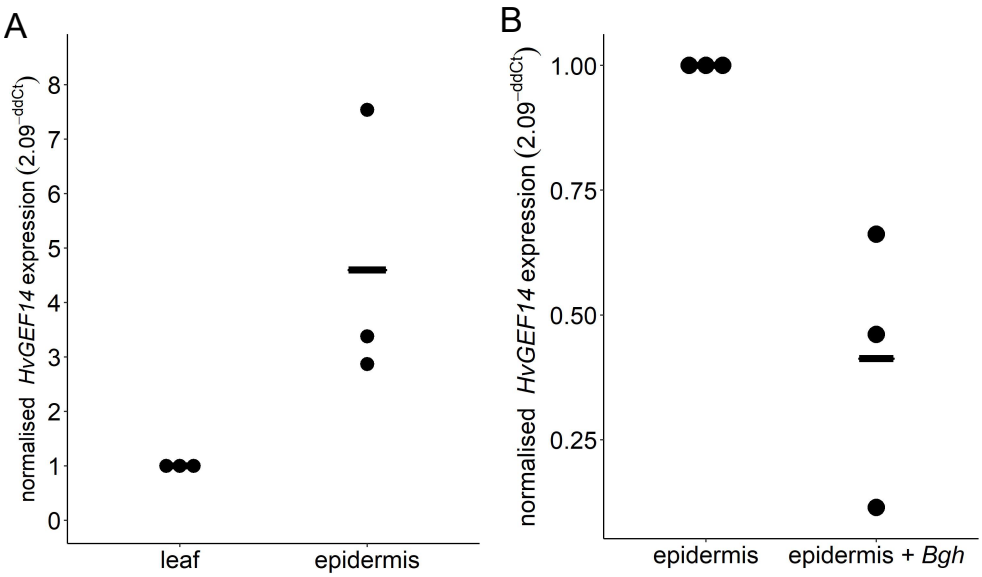

Fig. 3: ***HvGEF14* shows increased expression in epidermal peels and downregulation after inoculation with fungal spores.** *HvGEF14* is expressed in barley epidermis (A) and downregulated after Bgh inoculation (1 dpi) (B) in three independent repetitions (plants harvested on different days). Foldchange expression was calculated with primer efficiency correction and the 2^(-ddCt) method by Livak and Schmittgen (2001) and normalised to transcript levels in whole leaves (A) and non- inoculated epidermis (B).

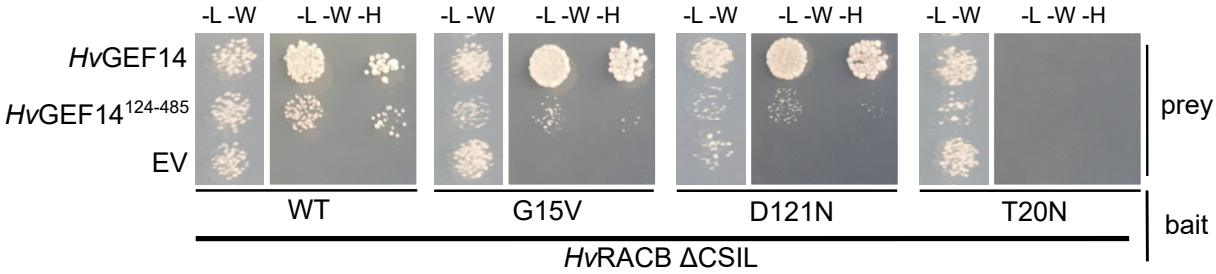

Fig.4: ***Hv*GEF14 interacts with barley ROP variants in yeast**. *Hv*RACB wild type (WT), G15V constitutively activated (CA), T20N dominant negative (DN) and D121N low nucleotide affinity variants were tested as bait against prey constructs *Hv*GEF14 full length, *Hv*GEF14 amino acids 124-485 (PRONE domain) or empty vector (EV). Interaction of proteins shown on media containing amino acid mix without leucine (L), tryptophan (W) and histidine (H), (-L-W-H) in two dilutions (factor 10^{-1}) to identify growth of single yeast colonies. Representative image of three experiments with the same result. Successful yeast transformation was confirmed with selective media (amino acid mix without leucine (L) and tryptophan (W) (-L-W). Dropout was performed on one -L-W and one -L-W-H plate and images were cropped during figure preparation for better visibility. Original images can be found in Fig. S1 (Fig. S4).

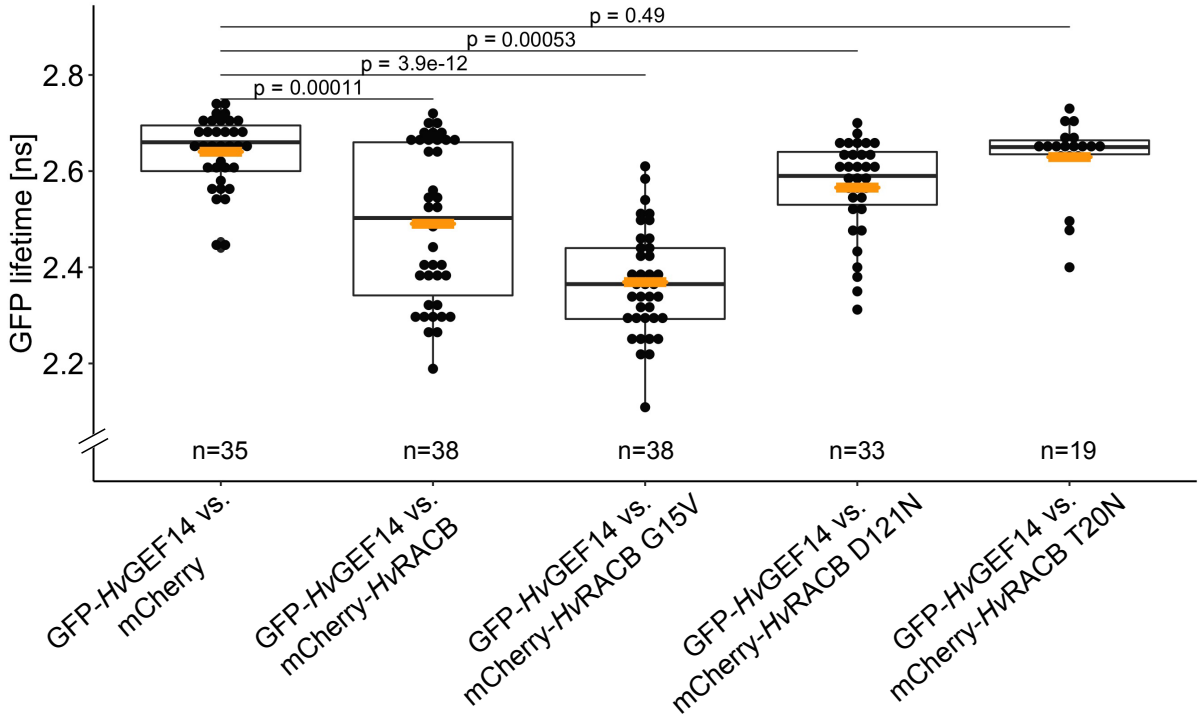

Fig. 5: ***Hv*GEF14 interacts with HvRACB variants in planta**. GFP-tagged *Hv*GEF14 full length was observed in FRET-FLIM experiments to interact with mCherry-tagged *Hv*RACB wild type (WT), constitutively activated (G15V) and low nucleotide affinity mutant (D121N) but not with dominant negative (T20N) RACB. Mean GFP lifetime is indicated with black point, n = number of cells observed in three independent experiments. Mean shown as orange dot. Kruskal-Wallis p-value = 4.346e-14, pairwise comparison was performed via wilcoxon test and bonferroni adjustment for multiple testing. (Rstudio, version 1.2.5033).

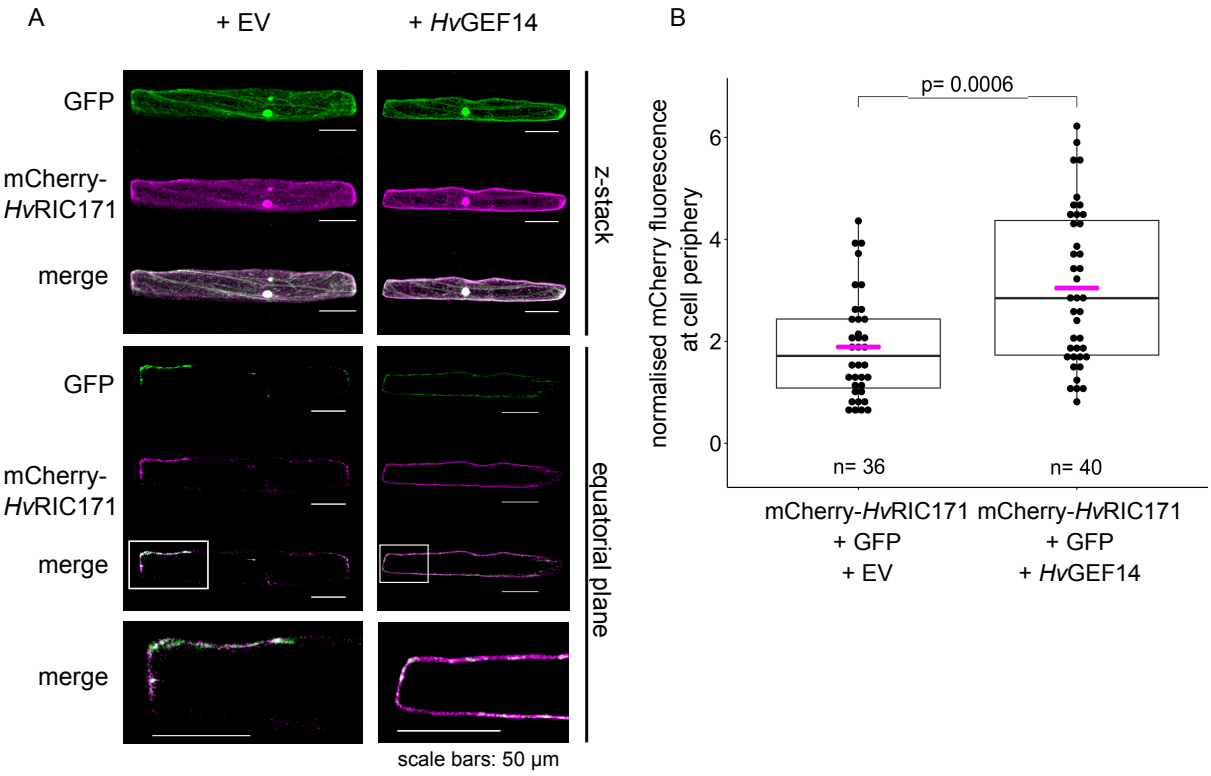

Fig. 6: ***Hv*GEF14 influences subcellular localisation of mCherry-*Hv*RIC171**. Localisation of mCherry-*Hv*RIC171, a downstream interactor of activated ROPs in barley, shows higher fluorescence intensity at the cell periphery when *Hv*GEF14 is co-expressed simultaneously. (A) Representative images of three biological replicates show z-stack and equatorial plane of mCherry-*Hv*RIC171 and cytosolic GFP fluorescence of transiently transformed barley epidermis cells. (B) Quantification of periphery mCherry fluorescence intensity normalized to whole cell mCherry and GFP fluorescence intensity measured in minimum 30 cells via Fiji, statistical analysis performed in Rstudio via wilcox test (Rstudio *version 1.2.5033*).

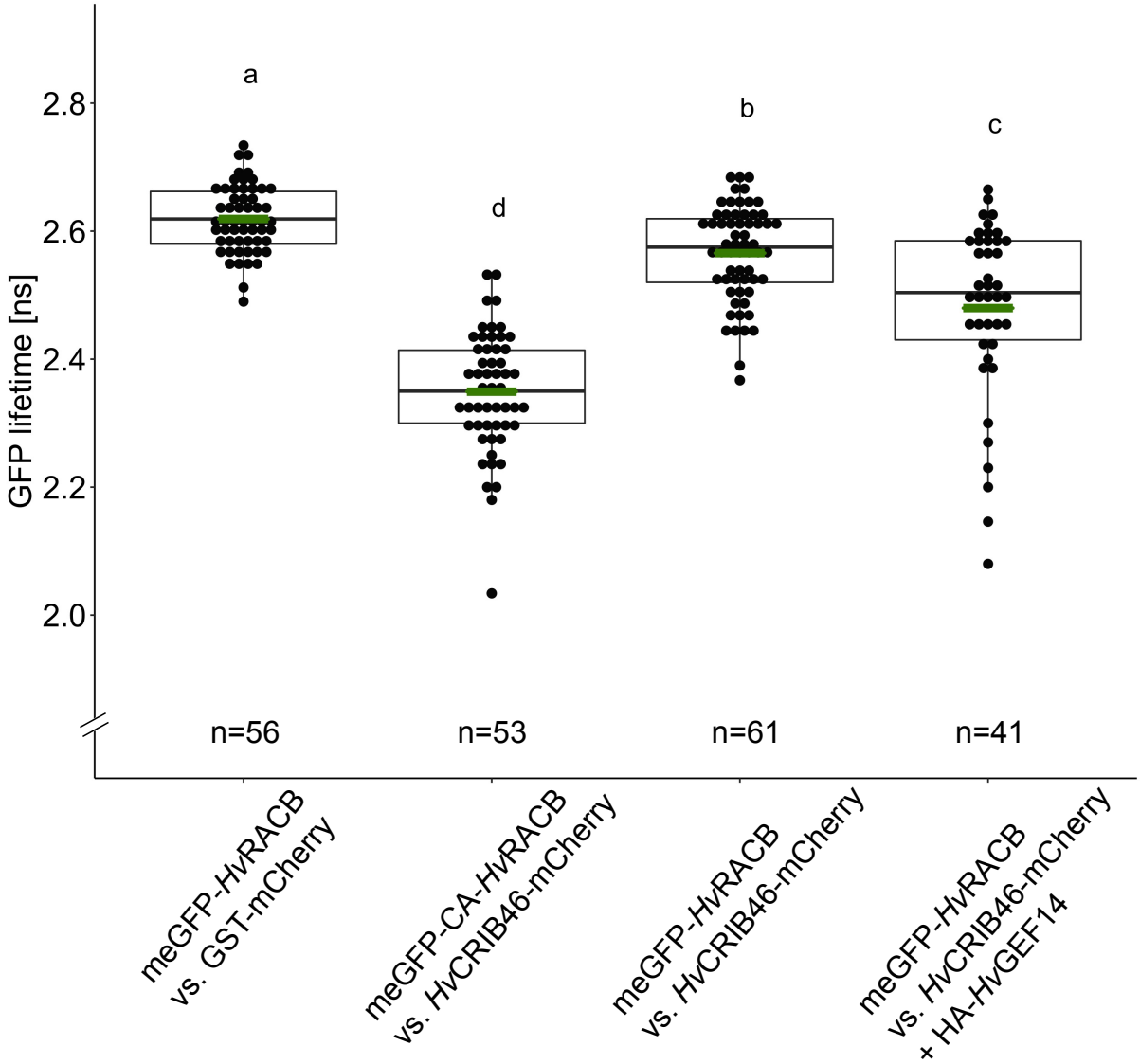

Fig. 7: ***Hv*RACB can be activated by *Hv*GEF14.** meGFP-*Hv*RACB interacts with *Hv*CRIB46-mCherry, a 46 amino acid fragment of *Hv*RIC171, when mutated (G15V) to a constitutively activated variant or in presence of *Hv*GEF14 during FRET-FLIM measurements in *N. benthamiana*. GST-mCherry used as negative control. Summary of six independent repetitions, Kruskal-Wallis comparison of means performed in Rstudio (version 1.2.5033) after testing for distribution of data.

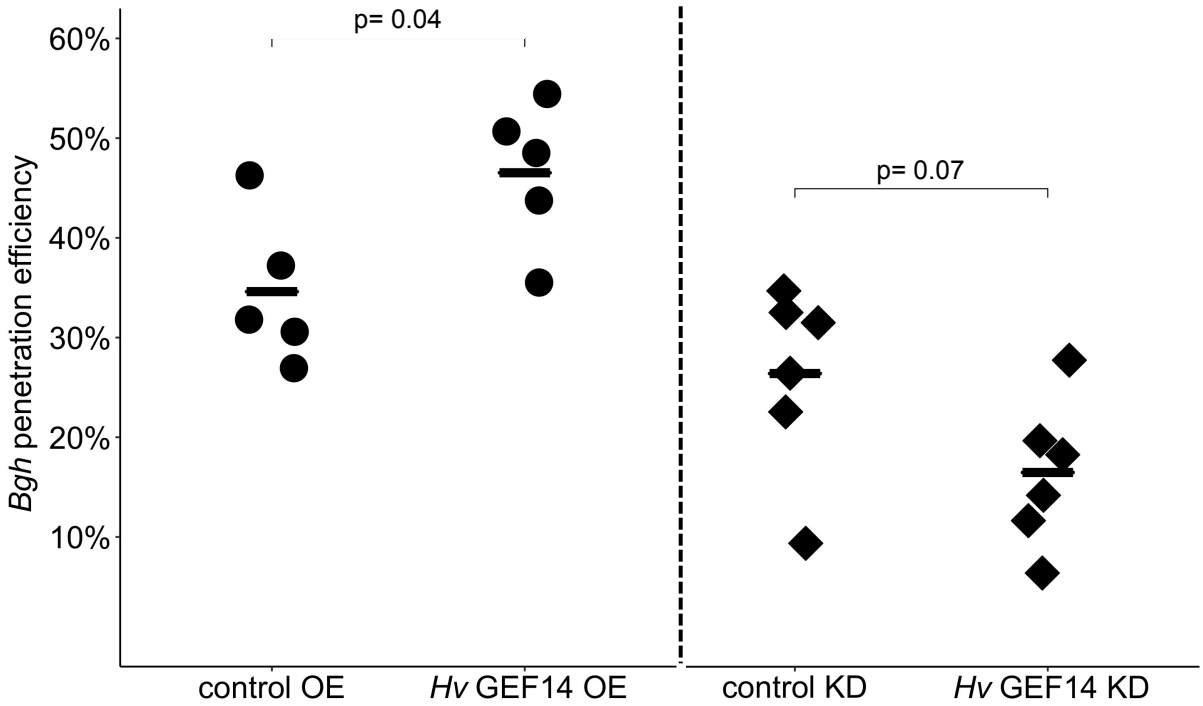

Fig. 8: ***Hv*GEF14 affects *Bgh* penetration efficiency.** *Bgh* penetration efficiency in barley epidermis cells over-expressing (OE) *Hv*GEF14 full length compared to mean penetration efficiency in cells with pGY1 empty vector (control OE) or after knock-down (KD) of *HvGEF14* via RNAi compared to mean penetration efficiency of pIPKTA30N empty vector (control KD). Mean values indicated with bar. Statistical significance of differences of the mean calculated with t-test in Rstudio (version 1.2.5033) after assessing for normal distribution with Shapiro-Wilk test.